Inorganic Chemistry

Article

pubs.acs.org/IC

Magnetic Resonance Properties of Actinyl Carbonate Complexes and Plutonyl(VI)-tris-nitrate

Frédéric Gendron,[†] Ben Pritchard,[†] Hélène Bolvin,[‡] and Jochen Autschbach*,[†]

[†]Department of Chemistry, University at Buffalo, State University of New York, Buffalo, New York 14260-3000, United States

[‡]Laboratoire de Physique et de Chimie Quantiques, Universite Toulouse 3, 118 Route de Narbonne, 31062 Toulouse, France

Supporting Information

ABSTRACT: Electronic structures and magnetic properties of actinyl ions AnO_2^{n+} (An = U, Np, and Pu) and the equatorially coordinated carbonate complexes $[UO_2(CO_3)_3]^{5-}$, $[NpO_2(CO_3)_3]^{4-}$, and $[PuO_2(CO_3)_3]^{4-}$ are investigated by ab initio quantum chemical calculations. The complex $[PuO_2(NO_3)_3]^-$ is also included because of experimentally available *g*-factors and for comparison with a previous study of $[NpO_2(NO_3)_3]^-$ (*Chem.—Eur. J.* **2014**, *20*, 7994-8011). The results are rationalized with the help of crystal-field (CF)-type models with parameters extracted from the ab initio calculations, and with the help of natural orbitals and natural spin orbitals contributing to the magnetic properties and the unpaired spin distribution, generated from the spin−orbit wave functions. These orbitals resemble textbooklike representations of the actinide 5f orbitals. Calculated paramagnetic susceptibilities are used to estimate dipolar ^{13}C chemical shifts for the carbonate ligands. Their signs and order of magnitude are compared to paramagnetic effects observed experimentally in NMR spectra. The results indicate that the experimental spectra are also influenced by contact shifts.

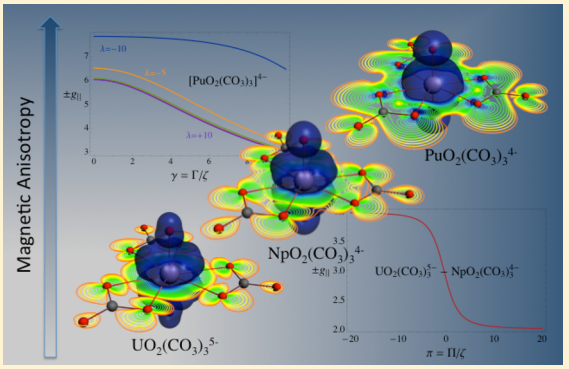

1. INTRODUCTION

The chemical and physical properties of the heaviest elements, actinides[1−4] (and transactinides), are very actively researched for a number of reasons. First, these elements are fascinating due to the involvement of 5f orbitals in new and unusual bonding scenarios.[5−7] Second, there are promising potential applications of 5f elements, for example in single-molecule magnets (SMMs).[8] Third, there exists a practical need to study, characterize, understand, and monitor the properties of 5f elements in the nuclear energy fuel cycle[9,10] and their chemical reactions in the environment[11] Despite many years of combined theoretical and experimental efforts, there are still large gaps in our understanding of the properties of 5f element compounds. Because of experimental difficulties related to radioactivity and toxicity, quantum chemistry plays an important role in this area of research.[12−14]

Of particular interest are the magnetic properties of actinide (An) compounds with unpaired electrons. The interplay of crystal-field (CF) splitting, spin−orbit (SO) coupling, and covalency involving the 5f shell dictates the resulting magnetic behavior and is of fundamental importance.[5] The electron paramagnetism can also be utilized in the experimental characterization of An complexes by magnetic resonance techniques, for instance, in electron paramagnetic resonance (EPR) and nuclear magnetic resonance (NMR) experiments. On the theory side, reliable ab initio calculations of the magnetic properties of actinide complexes are not trivial due to the need of relativistic quantum chemistry methods[15,16] that are capable of treating open-shell systems. We mention prior studies of the octahedral $5f^1$ series AnX_6^{n-} (X = halide) and selected $5f^3$ An^{III} complexes[17−27] where density functional theory (DFT) and/or complete active space (CAS) wave function methods have been applied successfully to calculate magnetic properties.

Actinyl (AnO_2^{n+}) carbonate complexes[28] form in aqueous solutions in contact with air.[9] Such complexes are thought to be one of the important forms in which actinide species originating from nuclear waste migrate to the environment.[9] Therefore, the properties of actinyl carbonate complexes are important subjects of research. Solution-phase NMR has been used in order to investigate the speciation of An carbonate complexes.[9,29] Open-shell actinyl complexes with U(V), Np(VI), and in particular Pu(VI), exhibit significant paramagnetic effects on the carbonate ^{13}C NMR chemical shifts in contrast to analogous diamagnetic uranyl(VI) systems. In the present study, we investigate the paramagnetism of tris-carbonate complexes of open-shell actinyl species and an analogous nitrate complex.

Recently,[30] we explored a combination of CAS and DFT methods to calculate the magnetic properties of the $5f^1$ system neptunyl(VI), NpO_2^{2+}, and two experimentally characterized complexes of neptunyl, viz., $[NpO_2(NO_3)_3]^-$ and $[NpO_2Cl_4]^{2-}$. The EPR *g*-factors of the latter two systems were successfully modeled by CAS calculations, both for the electronic ground states and several excited states. DFT was shown to give

Received: May 20, 2014
Published: July 30, 2014

   dx.doi.org/10.1021/ic501168a | *Inorg. Chem.* 2014, 53, 8577−8592

acceptable *g*-factors as well, but the calculations did not always converge to an electron density and magnetization density corresponding to the correct ground state and in some cases suffered from a spin-contamination-like problem. A thorough understanding of the chemical and magnetic properties of NpO_2^{2+} and the two complexes was derived from CF models extracted from the CAS results in combination with visualizations of spin-magnetization densities and natural orbitals for the electron density and spin magnetization generated from wave functions including SO coupling.

Herein, we apply these techniques to investigate the magnetic properties of UO_2^{+} ($5f^1$), NpO_2^{2+} ($5f^1$), and PuO_2^{2+} ($5f^2$), and carbonate complexes thereof, as shown schematically in Figure 1.

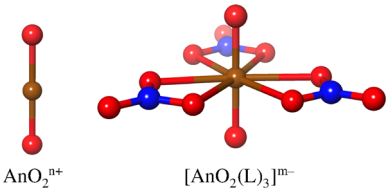

Figure 1. Actinyl ions AnO_2^{n+} with U(V) ($5f^1$, $n = 1$), Np(VI) ($5f^1$, $n = 2$), and Pu(VI) ($5f^2$, $n = 2$), tris-carbonate complexes ($m = 6 - n$), and $[PuO_2(NO_3)_3]^-$ ($m = 1$).

The $5f^2$ complex $[PuO_2(NO_3)_3]^-$ is also included in the present study because experimental EPR *g*-factors are available for further validation of the calculations. It is shown that trends for the natural orbital occupations directly connect qualitative information obtained from the CF models with quantitative information from ab initio expectation values for spin and orbital angular momenta and the calculated EPR *g*-factors, thereby providing a chemically intuitive analysis of the electronic structures of the complexes. Calculated van Vleck susceptibilities are further used to estimate the "through-space" dipolar contribution to the paramagnetic effects observed in the ^{13}C NMR spectra of actinyl carbonate complexes. We show that the signs and orders of magnitude of the dipolar shifts are consistent with experiment, but that quantitative modeling of the paramagnetic effects on the NMR shifts will require calculating accurate spin density distributions in the ligand systems.

Computational and theoretical details are provided in section 2. The results are analyzed and discussed in section 3, starting with the optimized structures, followed by CF models, assignments of the ground state and selected low-energy excited electronic states, *g*-factor calculations, analysis of the electronic structure of the ground states in terms of natural orbitals, and estimates of the dipolar ^{13}C chemical shifts. Concluding remarks and an outlook can be found in section 4.

2. COMPUTATIONAL AND THEORETICAL DETAILS

The computational protocol employed in this work is similar to the one developed for our recent work[30] on NpO_2^{2+} and therefore only briefly summarized here. Structure optimizations were performed using Density Functional Theory (DFT) with a 2012 version of the Amsterdam Density Functional (ADF) package.[31−33] The open metal shells were in some cases treated with fractional orbital occupations resembling an "average of configurations" (AOC).[34] The optimizations utilized the scalar relativistic all-electron zeroth-order regular approximation (ZORA) Hamiltonian,[35] the B3LYP[36] functional, and a triple-ζ doubly polarized all-electron Slater type basis (TZ2P) from the ADF basis set library. Solvent effects where included via the Conductor-Like Screening Model (COSMO) as implemented in ADF,[37] with parameters for water, because the experimental NMR data for the carbonate complexes were obtained in aqueous solution.

Wave-function-based electronic structure calculations were carried out with a 2013 developer's version of the Molcas code.[38] The 2nd-order Douglas−Kroll−Hess scalar Hamiltonian[39] was employed in the calculations without SO coupling, along with all-electron ANO-RCC Gaussian-type basis sets contracted to TZP quality (U, Np, Pu = 26s23p17d13f5g3*h*/9s8p6d4f2g1h; N, C, O = 14s9p4d3f2*g*/4s3p2d1f). The computations used state averaged CASSCF (Complete Active Space Self Consistent Field),[40] with inclusion of dynamical electron correlation by CASPT2 (Complete Active Space Perturbation Theory at second order).[41] SO coupling was treated by state interactions between the CASSCF/PT2 wave functions, using the RASSI (Restricted Active Space State Interaction) program.[42] The SO operator matrix was calculated from atomic mean-field (AMFI) SO integrals.[43] For brevity, scalar or "spin-free" (SF, i.e. non-SO) and SO CASSCF and CASPT2 calculations are occasionally referred to as SCF-SF, SCF-SO, PT2-SF, and PT2-SO. To reduce potential symmetry breaking, we employed "single-state" PT2 calculations where CASSCF wave functions are used to calculate the SO Hamiltonian, but PT2 energies are used for the diagonal elements. EPR *g*-factors were calculated according to ref 20.

A local modification[30,44] of Molcas was used to generate natural orbitals (NOs) and natural spin orbitals (NSOs) from SO RASSI calculations, and corresponding volume data for visualizations. Where appropriate, we employed linear combinations of the ground state Kramers doublet components diagonalizing the magnetic field component derivatives of the Zeeman Hamiltonian, after rotating the complexes such that their principal magnetic axes[45] coincided with the laboratory frame. In these calculations, real orthonormal NOs φ and NSOs φ_p^u were generated from the PT2-SO wave functions as eigenfunctions of the one-particle spin-free density matrix and the spin-magnetization density matrices, respectively, such that ($u = x$, y, or z)

$$\rho(\boldsymbol{r}) = \sum_p n_p[\phi_p(\boldsymbol{r})]^2 \quad \text{with} \sum_p n_p = N \tag{1a}$$

$$m^u(\boldsymbol{r}) = \sum_p n_p^u[\phi_p^u(\boldsymbol{r})]^2 \text{ with} \sum_p n_p^u = 2\langle S_u\rangle \tag{1b}$$

The numbers n_p and n_p^u show how much a given orbital contributes to the electron density $\rho(\boldsymbol{r})$ and to the unpaired spin distribution. The index p goes over the molecular orbital (MO) basis used in the calculation. N is the number of electrons, and $\langle S_u\rangle$ is the expectation value of the u component of the spin operator. Further, related to the expectation value as $\langle S_u\rangle = 1/2\int m^u(\boldsymbol{r})dV$, $m^u(\boldsymbol{r})$ is a component of the spin magnetization density. In a calculation without SO coupling and the usual choice of the spin quantization axis along z, the function m^z corresponds to the usual *spin density* $\rho^{\uparrow} - \rho^{\downarrow}$, whereas $m^x = 0$, $m^y = 0$. In the SO calculations this is not the case anymore, and the spin expectation values $\langle S_u\rangle$ may differ significantly from integer or half-integer values. In order to combine the information from all components of the spin magnetization, in section 3.6 we show plots of the noncollinear spin density,[46] which is given by

$$s(\boldsymbol{r}) = (m^x(\boldsymbol{r})^2 + m^y(\boldsymbol{r})^2 + m^z(\boldsymbol{r})^2)^{1/2} \tag{2}$$

Graphical visualizations of the components $m^u(\boldsymbol{r})$, $s(\boldsymbol{r})$, and the NOs and NSOs were created with the graphical user interface of the ADF suite. In some cases, due to slight symmetry breaking in the CASPT2 calculations, the reported spin and angular momentum expectation values and associated n_p and n_p^z values for pairs of degenerate orbitals have been averaged.

3. RESULTS AND DISCUSSION

3.1. Structures and Ligand-Binding Energies. The structures of the free actinyl complexes UO_2^{+}, NpO_2^{2+}, PuO_2^{2+} and the equatorially coordinated systems $[UO_2(CO_3)_3]^{5-}$, $[NpO_2(CO_3)_3]^{4-}$, $[PuO_2(NO_3)_3]^-$, and $[PuO_2(CO_3)_3]^{4-}$ were optimized with DFT. The optimized distances are given in Table 1 and are compared to experimental data where available. The latter were derived from EXAFS measurements. Different occupation schemes for the relevant 5f orbitals using integer and

dx.doi.org/10.1021/ic501168a | *Inorg. Chem.* 2014, 53, 8577−8592

Table 1. Comparison of Optimized Distances (Å), B3LYP-COSMO[a]

complex	An−O_{yl}	An−O_{eq}	An−C/N	An−O_{dist}	occup	ref
NpO_2^{2+}	1.712				$\phi_u^{0.5}\phi_u^{0.5}$	
$[NpO_2(CO_3)_3]^{4-}$	1.812	2.454	2.905	4.164	$\phi_{A'1}^1$	
	(1.79)	(2.45)	(2.90)	(4.18)		47
UO_2^+	1.809				$\phi_u^{0.5}\phi_u^{0.5}$	
$[UO_2(CO_3)_3]^{5-}$	1.916	2.546	2.986	4.258	$\phi_{A'1}^1$	
	(1.91)	(2.50)	(2.93)	(4.23)		48, 49
PuO_2^{2+}	1.682				$\delta_{E''}^1\delta_{E''}^1$	
$[PuO_2(CO_3)_3]^{4-}$	1.780	2.461	2.910	4.170	$\delta_{E''}^1\delta_{E''}^1$	
	(1.75)	(2.44)	(2.89)	(4.19)		9
$[PuO_2(NO_3)_3]^-$	1.737	2.491	2.932	4.143	$\delta_{E''}^1\delta_{E''}^1$	

[a]Different orbital occupations were used for the structure optimizations. For details, see Table S1 in the SI. Available experimental data from EXAFS measurements in parentheses.

fractional occupation have been explored in the DFT calculations; see Table S1 in the Supporting Information (SI) for details. We use the symmetry species σ, π, δ, ϕ of the $D_{\infty h}$ point group for the free actinyl ions to label the different 5f orbitals. Of prime concern here are the nonbonding 5f orbitals of δ and ϕ symmetry.

It was pointed out previously[50] that DFT can produce ground state geometries for actinide complexes in reasonable agreement with correlated wave function calculation. The ground state for the $5f^1$ free neptunyl NpO_2^{2+} moiety is in DFT best described by fractional occupations where the unpaired electron is shared by the two degenerate ϕ_u 5f orbitals, because of the orbital degeneracy of the SF $^2\Phi$ ground state. The DFT energy corresponding to a $^2\Delta$ configuration is close. Due to the fractional occupation setup, the relative energies of different configurations may not reflect the correct state ordering, but it is useful for the geometry optimizations. For free uranyl UO_2^+, the lowest DFT energy is for equal fractional occupations of the δ_u orbitals, with a configuration corresponding to $^2\Phi$ very close in energy. We selected the optimized $\phi_1^{0.5}\phi_2^{0.5}$ configuration for compatibility with free NpO_2^{2+}. In either case, the nonbonding nature of the ϕ and δ orbitals means that the impact on the An−O_{yl} bond lengths for varying occupations is relatively minor, as seen in the data collection in Table S1. There are no experimental structure data for the free actinyl ions available. The Np−O_{yl} and U−O_{yl} equilibrium distances are compatible with theoretical data previously reported in the literature, where Np−O_{yl} = 1.65−1.71 Å,[51,52] and U−O_{yl} = 1.74−1.77.[53,54]

The lowest DFT energies of the equatorially coordinated $[NpO_2(CO_3)_3]^{4-}$ and $[UO_2(CO_3)_3]^{5-}$ correspond to full occupations for one of the ϕ orbitals, because the lowering of the symmetry from $D_{\infty h}$ to D_{3h} lifts the ϕ-degeneracy as discussed in more detail in section 3.2. The computed bond distances for the two tris-carbonato actinyls are in fairly good agreement with experimental EXAFS data. The An−O_{yl} bond length is slightly overestimated by 0.01 and 0.02 Å in the neptunyl and the uranyl systems, respectively. A similar agreement between the computed and measured distances is found for the equatorial ligands where the largest deviation is found for the terminal An−O_{eq} distances which are overestimated by 0.05 Å in the DFT calculations. The DFT optimized structures can be compaired to previous optimizations performed at the CASPT2 level of theory for these two complexes. $[NpO_2(CO_3)_3]^{4-}$ has been optimized at the CAS(13/13)PT2 level of theory by Gagliardi et al.[55] A good agreement with experiment was found for the Np−O_{yl} bond length (1.805 Å); however, the distances of the equatorial ligands were overestimated (Np−O_{eq} = 2.533 Å, Np−C = 2.979 Å, and Np−O = 4.305 Å). A similar trend was found for $[UO_2(CO_3)_3]^{5-}$. U−O_{yl} bond distances of 1.898 and 1.929 Å were computed at the CASPT2 level,[53,54] but in both cases, the U−O_{eq} bond lengths were overestimated (2.603 and 2.529 Å).

The lowest-energy DFT results for PuO_2^{2+} and the complexes $[PuO_2(NO_3)_3]^-$ and $[PuO_2(CO_3)_3]^{4-}$ correspond to configurations where the two unpaired electrons occupy the degenerate 5f δ orbitals (corresponding to the spectroscopic term $^3\Sigma^-$). According to Hund's rules, this differs from the expected ^3H ground state where the unpaired electrons occupy δ and ϕ orbitals. This behavior of scalar relativistic DFT was already noted in studies of AnO_2^{n+} ions.[56,57] In a multireference calculation, the $^3\Sigma^-$ term arises from a mixture of the two configurations δ^2 and ϕ^2. A single-reference Kohn−Sham DFT calculation with integer orbital occupations cannot mix these configurations. Nonetheless, for the plutonyl carbonate complex the DFT optimized bond distances are in good agreement with the EXAFS data. The largest difference is found for the Pu−O_{yl} distance which is overestimated by 0.05 Å, while the Pu−L_{eq} distances are overestimated by 0.02 Å. The computed distances for the plutonyl nitrate complex are compatible with those found in the literature. Odoh et al. recently optimized $[PuO_2(NO_3)_3]^-$ at the DFT level of theory (B3LYP/RECP/aug-cc-pVTZ).[58] In aqueous solution (PCM model), the computed Pu−O_{yl} and Pu−O_{eq} distances were 1.737 and 2.483 Å.

As already pointed out in our previous work[30] and related literature, in the equatorially coordinated complexes, the An−O_{yl} distances are lengthened relative to the free actinyl ions. Indeed, the presence of the equatorial ligands leads both to a decrease of the electronic population in the bonding An−O_{yl} σ and π orbitals and to an increase of the electrostatic repulsion between the O_{yl} atoms and the equatorial ligands.[53,59] The lengthening of the An−O_{yl} bonds is found to be more pronounced in the carbonate systems studied herein than in the analogous nitrate complexes. For instance, the Np−O_{yl} bond length goes from 1.712 Å in the free neptunyl to 1.789 and 1.812 Å in $[NpO_2(NO_3)_3]^-$ and $[NpO_2(CO_3)_3]^{4-}$, respectively. A similar trend is computed for plutonyl where the Pu−O_{yl} bond lengthens from 1.682 Å to 1.737 and 1.780 Å in the nitrate and carbonate systems, respectively. These trends show that a stronger interaction takes place between the equatorial carbonate ligands and the actinyl ions than that with the nitrate ligands.

The interactions between the actinyl ions and their equatorial ligands were investigated with the help of a Morokuma−Ziegler−Rauk bond energy decomposition.[60,61] In this decomposition scheme, the binding energy ΔE_{BE} between two fragments, in our case AnO_2^{2+}

dx.doi.org/10.1021/ic501168a | Inorg. Chem. 2014, 53, 8577−8592

(An = Np and Pu) and the equatorial ligand system $(NO_3)_3^{3-}$ or $(CO_3)_3^{6-}$, is split into three types of interactions as follows:

$$\Delta E_{BE} = \Delta E_{Elec} + \Delta E_{Pauli} + \Delta E_{Orb}$$

Here, ΔE_{Elec}, ΔE_{Pauli}, and ΔE_{Orb} correspond to the electrostatic interaction, Pauli repulsion, and the orbital interaction, respectively. Results of this analysis for $[NpO_2(NO_3)_3]^-$, $[NpO_2(CO_3)_3]^{4-}$, $[PuO_2(NO_3)_3]^-$, and $[PuO_2(CO_3)_3]^{4-}$ are collected in Table 2. In line with the impact on the An−O_{yl} bond

Table 2. Binding Energy (eV) of AnO_2^{2+} with the Equatorial Ligand System L_3 (L = NO_3^-, CO_3^{2-}), B3LYP/TZ2P

	ΔE_{Pauli}	ΔE_{Orb}	ΔE_{Elec}	ΔE_{BE}
$[NpO_2(NO_3)_3]^-$	8.19	−9.69	−33.51	−35.01
$[NpO_2(CO_3)_3]^{4-}$	11.02	−13.04	−61.81	−63.83
$[PuO_2(NO_3)_3]^-$	7.81	−9.57	−33.21	−34.97
$[PuO_2(CO_3)_3]^{4-}$	10.16	−12.51	−61.02	−63.37

distances, the binding energy increases by roughly a factor of 2 when replacing the nitrate ligands by carbonate. In all cases, the orbital contribution and the Pauli repulsion have roughly the same magnitudes and cancel to a large degree, leaving the electrostatic components as the dominant ones and the one responsible for the increase of the binding energy from nitrate to carbonate. This result is expected because the carbonate ligands carry twice the formal charge.

3.2. Crystal-Field Models. In a previous paper on NpO_2^{2+}, we showed that the nature and the ordering of electronic states in the 5f manifold, and hence the magnetic properties, can be rationalized with the help of a simple model combining crystal-field (CF) and spin−orbit (SO) interactions.[30] We apply a similar model here, and we further extend it to the effective two-electron PuO_2^{2+} case.

The model Hamiltonian corresponds to a one-electron operator combining the CF and SO effects: $\hat{H}^m = \hat{H}^{SO} + \hat{H}^{CF}$. The one-electron SO operator takes the form $\hat{H}^{SO} = \zeta\hat{\boldsymbol{L}}\cdot\hat{\boldsymbol{S}}$ with a semiempirical SO coupling constant ζ and the orbital and spin angular momentum vector operators $\hat{\boldsymbol{L}}$ and $\hat{\boldsymbol{S}}$. A scalar CF operator models the interaction with the ligands. In this work, the CF parameters and the SO coupling constant are extracted from the ab initio calculations. Therefore, the model parameters not only describe electrostatic crystal-field effects but also incorporate some covalent interactions to the extent that they can be parametrized by the model Hamiltonian.

In the following, the states are described in a basis of spin-free $l = 3$ angular momentum and spin $s = 1/2$ atomic orbitals characterized by the projection quantum numbers, $|m_l,m_s\rangle$. Only the angular part of the orbitals is specified explicitly. The shapes and extensions of the radial functions are implicitly included in the models via the parameters extracted from the ab initio calculations. The symmetry labels σ, π, δ, and ϕ correspond to the angular momentum projections $m_l = 0, \pm 1, \pm 2$ and ± 3, respectively. Because SO coupling is a strong interaction for actinides, it is sometimes easier to describe the CF interaction in terms of atomic spinors $|j,m_j\rangle$, where $j = l \pm s$ is the total angular momentum and m_j its projection onto the quantization axis (see Table S9 in the SI regarding the composition of the $|j,m_j\rangle$ spinors in terms of spherical harmonics and spin functions).

In the case of the plutonyl complexes, the two-electron states are characterized by spectroscopic term denoted as $^{2S+1}(M_L)_{\pm J}$, where M_L is the total angular momentum projection $M_L = \sum m_l$. In the $D_{\infty h}$ symmetry point group, the spectroscopic terms are often given as $^{2S+1}\Lambda_{\Omega(g/u)}$, where Λ and Ω are the projections of the orbital L and total J angular momenta onto the internuclear axis, and defined as $\Lambda = |M_L|$ and $\Omega = \Lambda + M_S$. When the symmetry is lowered from linear to D_{3h} for the carbonate and nitrate complexes, these are not proper quantum numbers anymore. However, it is sometimes easier to refer to a state of one of the D_{3h} systems in terms of the dominant contribution from the $D_{\infty h}$ *parent* symmetry, which we frequently do in the following discussion.

3.2.1. Uranyl and Neptunyl 5f^1. In the free actinyl ions AnO_2^{n+}, the ligand field interaction between the actinide center and the O_{yl} atoms leads to the formation of strong An−O_{yl} formal triple bonds. The 5f σ_u and π_u orbitals form bonding and antibonding combinations with the oxygen 2*p* orbitals, whereas the 5f δ_u and ϕ_u orbitals remain formally nonbonding.[30,62,63] The SO interaction can mix orbitals of δ_u and ϕ_u symmetry. Therefore, the 5f^1 electronic configuration of the AnO_2^{n+} ions is described mainly by an admixture of the 5f δ_u and ϕ_u orbitals. Accordingly, a simple model wave function can be set up with this set of orbitals. The δ_u orbitals, in which the electron density maxima are slightly shifted toward the oxygen atoms, are destabilized by the axial crystal-field. The SF ground state is therefore of spin-free $^2\Phi_u$ parentage where the unpaired electron is described by the two degenerate ϕ_u orbitals and the electron density is spread out in the equatorial plane as far away from the An−O_{yl} bonds as possible. Upon considering the SO interaction, the spin-free ground-state $^2\Phi_u$ then mixes with the low-energy spin-free $^2\Delta_u$ excited state. One may also consider the SO interaction first and consider the presence of the ligands via mixing of $|j,m_j\rangle$ atomic spinors. The actinyl 5f^1 ground state is then of $|5/2, \pm 5/2\rangle$ parentage,[30,62] with orbital angular momentum $l = 3$, $m_l = \pm 3$ and spin angular momentum $m_s = \mp 1/2$ antiparallel. Because of the lowering of symmetry from spherical to linear in the actinyl ions, the $|5/2, \pm 5/2\rangle$ ground state can mix with $|7/2, \pm 5/2\rangle$, while m_j remains a good quantum number.

Table 3 lists the model wave functions $|\psi\rangle$ for AnO_2^{n+}. The Kramers conjugates of the wave functions, $|\overline{\psi}\rangle$, are also listed, because they are needed to calculate the *g*-factors perpendicular to the main magnetic axis. The model Hamiltonian, shown in Equation S1 in the SI, contains a CF parameter Λ to reproduce the energetic splitting between the δ_u and ϕ_u orbitals, and the SO coupling constant ζ. The eigenfunctions depend on the reduced CF parameter $\lambda = \Lambda/\zeta$ and are given by real coefficients *A* and *B* describing the mixing of different $|m_l,m_s\rangle$. The result can be converted to the $|j,m_j\rangle$ basis with real coefficients *a* and *b*. The *g*-factors produced by the model wave functions are also given in Table 3. They were calculated as follows:

$$g_{\parallel} = 2\langle\psi|\hat{L}_z + g_e\hat{S}_z|\psi\rangle$$

$$g_{\perp} = 2\mathrm{Re}\langle\overline{\psi}|\hat{L}_x + g_e\hat{S}_x|\psi\rangle$$

$$= 2\mathrm{Im}\langle\overline{\psi}|\hat{L}_y + g_e\hat{S}_y|\psi\rangle$$

using $g_e = 2$ as predicted by the Dirac equation. From the state energies and the state interaction energies in the CAS(7,10)PT2 calculations, we extract for the CF model the parameters listed in Table 4 for UO_2^+ and NpO_2^{2+}. The small values of *b* show that the ground states are very similar to the $|5/2, \pm 5/2\rangle$ function of a 5f^1 actinide ion, with only small admixtures of $|7/2, \pm 5/2\rangle$. The CF model predicts $g_{\parallel} = \pm 4.21$ and ± 4.22 for UO_2^+ and NpO_2^{2+}, respectively. The magnitude is close to the free-ion limit (Np^{6+}, U^{5+}) where for a pure $|5/2, \pm 5/2\rangle$ state $g_{\parallel} = \pm 4.29$. The CF models reproduce the *g*-factors of the ab initio calculation

dx.doi.org/10.1021/ic501168a | Inorg. Chem. 2014, 53, 8577−8592

Table 3. CF + SO Model: Kramers Doublet Components $|\psi\rangle$, $|\bar{\psi}\rangle$ for Free and Equatorially Coordinated $5f^1$ Systems Wavefunctions of a $\tilde{S} = 1/2$ Pseudo-Spin, and Resulting *g*-Factors[a]

UO_2^+/NpO_2^{2+}

$$|\psi\rangle = A\left|-3,+\tfrac{1}{2}\right\rangle + B\left|-2,-\tfrac{1}{2}\right\rangle \qquad g_{\parallel} = \mp(4A^2 + 6B^2)$$

$$= a\left|\tfrac{5}{2},-\tfrac{5}{2}\right\rangle + b\left|\tfrac{7}{2},-\tfrac{5}{2}\right\rangle \qquad = \mp\left(\tfrac{30}{7}a^2 + \tfrac{40}{7}b^2 - \tfrac{4\sqrt{6}}{7}ab\right)$$

$$|\bar{\psi}\rangle = -A\left|3,-\tfrac{1}{2}\right\rangle - B\left|2,+\tfrac{1}{2}\right\rangle \qquad g_{\perp} = 0$$

$$= -a\left|\tfrac{5}{2},+\tfrac{5}{2}\right\rangle - b\left|\tfrac{7}{2},+\tfrac{5}{2}\right\rangle$$

$[UO_2(CO_3)_3]^{6-}/[NpO_2(CO_3)_3]^{4-}$

$$|\psi\rangle = A\left|-2,+\tfrac{1}{2}\right\rangle + B\left|-1,-\tfrac{1}{2}\right\rangle \qquad g_{\parallel} = \mp(2A^2 + 4B^2)$$

$$= a\left|\tfrac{5}{2},-\tfrac{3}{2}\right\rangle + b\left|\tfrac{7}{2},-\tfrac{3}{2}\right\rangle \qquad = \mp\left(\tfrac{18}{7}a^2 + \tfrac{24}{7}b^2 - \tfrac{4\sqrt{10}}{7}ab\right)$$

$$|\bar{\psi}\rangle = A\left|2,-\tfrac{1}{2}\right\rangle + B\left|1,+\tfrac{1}{2}\right\rangle \qquad g_{\perp} = 0$$

$$= -a\left|\tfrac{5}{2},+\tfrac{3}{2}\right\rangle - b\left|\tfrac{7}{2},+\tfrac{3}{2}\right\rangle$$

[a] Coefficients are determined from the eigenvectors of the CF + SO model Hamiltonian. See Table 4 for numerical data. Real coefficients A and B for $|m_l,m_s\rangle$ functions, real coefficients a and b for $|j,m_j\rangle$. Normalization implies $A^2 + B^2 = a^2 + b^2 = 1$. The signs of the m_j components for $|\psi\rangle$ and $|\bar{\psi}\rangle$ were chosen according to the discussion in ref 30.

Table 4. Parameters[a] for the CF + SO Models Derived from CAS(7,10)PT2 Calculations, and Resulting *g*-Factors[b]

	UO_2^+	NpO_2^{2+}	$[UO_2(CO_3)_3]^{5-}$	$[NpO_2(CO_3)_3]^{4-}$
ζ	1935	2304	2010	2374
Λ	1131	1327	−2204	−3199
Γ			3632	4947
Π	15 168	21 957	8112	12 413
A	0.944	0.944	0.967	0.976
B	−0.329	−0.330	−0.256	−0.218
a	0.998	0.998	0.954	0.941
b	0.052	0.051	0.299	0.337
$\pm g_{\parallel}$	4.216	4.218	2.131	2.095
$g_{\perp}$	0.000	0.000	0.000	0.000

[a] Parameters: ζ, Λ, Γ and Π in cm^{-1}. [b] See Table 3 for the wavefunction definitions and expressions for the *g*-factors.

well (see section 3.4), which serves as an internal consistency check. Regarding a discussion of the signs of the *g*-factor, the reader is referred to ref 30.

For the $5f^1$ carbonate complexes, the presence of the equatorial ligands lowers the symmetry to D_{3h} which means that m_j ceases to be a good quantum number. The CF interaction splits the degeneracy of the ϕ orbitals. Considering, first, a dominantly $|5/2, \pm 5/2\rangle$ actinyl ground state. The equatorial CF interaction mixes $|7/2, \mp 7/2\rangle$ and $|5/2, \pm 5/2\rangle$ orbitals. In the SF $|m_l,m_s\rangle$ framework, the new coupling is between $|\mp 3, \pm 1/2\rangle$ and $|\mp 3, \pm 1/2\rangle$. The model Hamiltonian corresponding to this model wave function is given in eq S3 of the SI. This model was previously used to reproduce the ab initio *g*-factors of a related neptunyl nitrate complex $[NpO_2(NO_3)_3]^-$.[30]

Using the CF parameters generated for a model for a $m_j = \pm 5/2$ parentage ground state gives $g_{\parallel} = 3.94$ and $g_{\perp} = 0.24$ for $[UO_2(CO_3)_3]^{5-}$ and $g_{\parallel} = 3.88$ and $g_{\perp} = 0.22$ for $[NpO_2(CO_3)_3]^{4-}$. These magnetic data strongly differ from the ab initio results for a simple reason: the ab initio calculations for $[UO_2(CO_3)_3]^{5-}$ and $[NpO_2(CO_3)_3]^{4-}$ give *g*-factors corresponding to ground states of $^2\Delta$ parentage, involving dominantly δ_u orbitals, with $g_{\parallel} = 2.12$ and 2.07 for the uranyl and neptunyl complexes, respectively, and with $g_{\perp} = 0.01$ in both cases (see Table 8).

Indeed, in the carbonate complexes the destabilization of the ϕ orbitals is stronger than in the nitrate complex, which renders the $^2\Delta$ state at the SF level energetically favorable over $^2\Phi$. This is consistent with the stronger electrostatic interactions found for carbonate ligands (Table 2). In the $|j,m_j\rangle$ basis, the SO ground state is of $|5/2, \pm 3/2\rangle$ parentage. In the SF $|m_l,m_s\rangle$ framework, the SO coupling is between $|-2,+1/2\rangle$ and $|-1,-1/2\rangle$. A simple model Hamiltonian takes the form:

$\hat{H}^m/\zeta$	$\lvert -2,+\frac{1}{2}\rangle$	$\lvert -1,-\frac{1}{2}\rangle$
$\langle -2,+\frac{1}{2}\rvert$	-1	$\sqrt{\frac{5}{2}}$
$\langle -1,-\frac{1}{2}\rvert$	$\sqrt{\frac{5}{2}}$	$\frac{1}{2} + \pi$

The off-diagonal elements of the Hamiltonian describe the SO coupling between δ and π 5f orbitals. A new CF parameter Π, with $\pi = \Pi/\zeta$, is introduced in the model to reproduce the energetic destabilization of the π orbitals relative to δ which impacts the extent of the SO mixing relative to the parent $|5/2, \pm 3/2\rangle$. Because the energetic destabilization of the π orbitals relative to δ is smaller for the carbonate complexes than for the free actinyl ions, the actinyl carbonate CF models benefit from attenuating the SO interaction between δ and π. In the subspace $m_j = \pm 3/2$, the CF parameter Γ responsible for the energetic splitting of the ϕ_u orbitals in the subspace $m_j = \pm 5/2$ is not used because the corresponding CF operator has no effect on the δ and π orbitals.

The associated wave functions and *g*-factors are listed in Table 3, and the parameters extracted for the model from the ab initio calculations are given in Table 4. The model for the $m_j = \pm 3/2$ subspace predicts $g_{\parallel} = 2.13$ and 2.09 for $[UO_2(CO_3)_3]^{5-}$ and $[NpO_2(CO_3)_3]^{4-}$, respectively, which is in excellent agreement with the ab initio data discussed below.

One can notice that the magnitude of $g_{\parallel}$ is consistent with weak SO coupling (i.e., it is quite small compared to the free-ion value for a $|5/2, \pm 3/2\rangle$ state ($g_{\parallel} = 2.57$)) because the parameter Π is on the order of 10^4 cm^{-1}. Indeed, the squares of the coefficients A and B of the model wave function, associated with $|-2,+1/2\rangle$ and $|-1,-1/2\rangle$, respectively, give ratios of SF $^2\Delta/^2\Pi$ of 93.5/6.5 and 95.3/4.7 for $[UO_2(CO_3)_3]^{5-}$ and $[NpO_2(CO_3)_3]^{4-}$, respectively. These ratios strongly differ from that of a $|5/2, \pm 3/2\rangle$ spinor (71/29).

3.2.2. Plutonyl $5f^2$. The paramagnetic properties of a series plutonyl complexes have been studied in the early 1950s by Eisenstein and Pryce (EP) who proposed a model to estimate the magnitude of the *g*-factors.[64] In a first approximation, EP considered that the ground state of the plutonyl ion is doubly degenerate and characterized by the spectroscopic term $^3H_{\pm 4}$ or $^3H_{4g}$, with a total angular momentum projection $M_L = \sum m_l = \pm 3 \pm 2 = \pm 5$ and the total spin angular momentum antiparallel to the orbital angular momentum. Indeed, as shown below at the SF level the two interacting unpaired 5f electrons equally occupy f_{δ} ($m_l = \pm 2$) and f_{ϕ} ($m_l = \pm 3$) orbitals with the same spin projections $\mp 1/2$ in order to balance the electron repulsion and

dx.doi.org/10.1021/ic501168a | Inorg. Chem. 2014, 53, 8577−8592

the CF effects. The total spin projection, $M_S = \mp 1/2 \mp 1/2 = \mp 1$, is antiparallel to the angular momentum projection $M_L = \pm 5$ such that in the EP model $g_{\parallel} = 2\langle\psi|\hat{L}_z + 2\hat{S}_z|\psi\rangle = \pm 6$.

The ground state wave function must also take into account SO coupling. The SO interaction can mix different states with the same $\Omega = 4_g$. For instance, $^3H_{4g}$ ($m_{l1} = \pm 3$, $m_{l2} = \pm 2$) can formally mix with $^3\Gamma_{4g}$ ($m_{l1} = \pm 3$, $m_{l2} = \pm 1$), $^3\Phi_{4g}$ ($m_{l1} = \pm 2$, $m_{l2} = \pm 1$) and $^1\Gamma_{4g}$ ($m_{l1} = \pm 2$, $m_{l2} = \pm 2$). In this work, the CF and SO parameters are extracted from ab initio calculations performed at the CAS(2,4)SCF level of theory. We use a minimal active space containing only δ and ϕ orbitals because it allows to analyze the main interactions in a simplified way. The contributions to the magnetic properties from states containing π orbitals (i.e., $^3\Gamma_{4g}$ and $^3\Phi_{4g}$) are shown to be small in section 3.4. Therefore, we consider a model in which the SO interaction mixes SF $^3H_{4g}$ ($m_{l1} = \pm 3$, $m_{l2} = \pm 2$) and $^1\Gamma_{4g}$ ($m_{l1} = \pm 2$, $m_{l2} = \pm 2$). In order to take the CF interaction with the equatorial ligands into account, we need to consider contributions from a state with ϕ orbitals of opposite m_l in order to allow for an energetic splitting of the ϕ orbitals. This state is $^3\Pi_{\mp 2}$ ($m_{l1} = \mp 3$, $m_{l2} = \pm 2$).

In summary, the CF model is set up in terms of two-electron wave functions, written here as Slater determinants in a shorthand notation, viz., $\left|a, b\right| = (1/2!)^{1/2}\det\begin{pmatrix}\psi_a(1), \psi_b(1)\\ \psi_a(2), \psi_b(2)\end{pmatrix}$ with ψ_a, ψ_b being $|m_l,m_s\rangle$ orbitals. The considered configurations are

$$|^3H_4\rangle = \left|\left|3, -\frac{1}{2}\right\rangle, \left|2, -\frac{1}{2}\right\rangle\right|$$

$$|^1\Gamma_4\rangle = \left|\left|2, \frac{1}{2}\right\rangle, \left|2, -\frac{1}{2}\right\rangle\right|$$

$$|^3\Pi_{-2}\rangle = \left|\left|-3, -\frac{1}{2}\right\rangle, \left|2, -\frac{1}{2}\right\rangle\right|$$

The model wave function for free PuO_2^{2+} is written as in Table 5, with real coefficients A and B describing the mixing of SF $^3H_{4g}$ and $^1\Gamma_{4g}$ under the SO interaction. The corresponding g-factors are also listed. The matrix representation for the model Hamiltonian is[65]

Table 5. CF + SO Model: Kramers Doublet Component $|\psi\rangle$ for Free and Equatorially Coordinated Plutonyl $5f^2$ Wavefunctions of a $\tilde{S} = 1/2$ Pseudo-Spin, and Resulting g-Factors[a]

PuO_2^{2+}	
$\|\psi\rangle = A\|^3H_{4g}\rangle + B\|^1\Gamma_{4g}\rangle$	$g_{\parallel} = \pm (6A^2+8B^2)$
$= A\left\|\left\|3, -\frac{1}{2}\right\rangle, \left\|2, -\frac{1}{2}\right\rangle\right\| + B\left\|\left\|2, \frac{1}{2}\right\rangle, \left\|2, -\frac{1}{2}\right\rangle\right\|$	$g_{\perp} = 0$
$[PuO_2(CO_3)_3]^{4-}/[PuO_2(NO_3)_3]^{-}$	
$\|\psi\rangle = A\|^3H_4\rangle + B\|^1\Gamma_4\rangle + C\|^3\Pi_{-2}\rangle$	$g_{\parallel} = \pm (6A^2+8B^2-6C^2)$
$= A\left\|\left\|3, -\frac{1}{2}\right\rangle, \left\|2, -\frac{1}{2}\right\rangle\right\| + B\left\|\left\|2, \frac{1}{2}\right\rangle, \left\|2, -\frac{1}{2}\right\rangle\right\|$	$g_{\perp} = 0$
$+ C\left\|\left\|-3, -\frac{1}{2}\right\rangle, \left\|2, -\frac{1}{2}\right\rangle\right\|$	

[a]Coefficients are determined from the eigenvectors of the CF + SO model Hamiltonian. Real coefficients A,B,C for $|m_l,m_s\rangle$ functions. Normalization implies $A^2+B^2+C^2 = 1$.

$\hat{H}^{CF} + \hat{H}^{SO}$	$\|^3H_{4g}\rangle$	$\|^1\Gamma_{4g}\rangle$
$\|^3H_{4g}\rangle$	$E(^3H_g) - \frac{5}{2}\zeta$	$\sqrt{\frac{3}{2}}\zeta$
$\|^1\Gamma_{4g}\rangle$	$\sqrt{\frac{3}{2}}\zeta$	$E(^1\Gamma_g)$

Here, ζ is the SO coupling constant used to set up $\hat{H}^{SO} = \zeta\sum_i \hat{L}(i)\,\hat{S}(i)$. Further

$$E(^3H) = \Lambda + J(3, 2) - K(3, 2)$$

$$E(^1\Gamma) = 2\Lambda + J(2, 2)$$

Here, $E(^3H)$ and $E(^1\Gamma)$ are the relative energies of the corresponding SF states. As in the case of the $5f^1$ systems discussed above, the CF parameter Λ describes the energetic splitting between the δ and ϕ orbitals. Because the plutonyl ion has two 5f electrons, the spin-free energies also include two-electron electron repulsion integrals (ERIs). In the model, the relevant Coulomb and exchange ERIs between 5f orbitals are denoted as $J(m_l, m_l')$ and $K(m_l, m_l')$, respectively. A fit of the CAS(2,4)SCF SF energies allowed to extract the values of the ERIs, as detailed in the SI. The fitting also gives $\Lambda = 3662$ cm^{-1} and $\zeta = 2663$ cm^{-1} for free PuO_2^{2+}, which places the δ orbitals at higher energy than ϕ consistent with the model for the f^1 systems. Nonetheless, the ground state has an electronic configuration $\phi^1\delta^1$, mainly due to the magnitudes of the Coulomb integrals $J(m_l, m_l')$ which order the electronic configurations as follows: $\phi^1\delta^1 < \delta^1\delta^1 < \phi^1\phi^1$ (see Equation S8a in the SI). Upon solving for the eigenvectors of the model Hamiltonian, the ground state wave function has only a small contribution of the SF $^1\Gamma_{4g}$ state (2%), resulting in a slightly raised magnitude of $g_{\parallel} = 6.04$ compared to $g_{\parallel} = 6$ exactly for the SF doublet $^3H_{4g}$. The former value agrees well with the ab initio result obtained at the CAS(2,4)SCF-SO level ($g_{\parallel} = 6.03$), confirming internal consistency of the CF model with the CAS calculation.

The top panel of Figure 2 shows the dependence of $g_{\parallel}$ in PuO_2^{2+} as a function of the reduced CF parameter $\lambda = \Lambda/\zeta$. For the limit of negligible SO coupling at some finite CF splitting, $\lambda = \pm\infty$, one finds $A = 1$, $B = 0$, or $A = 0$, $B = 1$, respectively. In this case, we have a SF $^3H_{4g}$ or $^1\Gamma_{4g}$ state, with $g_{\parallel} = 6$ or 8, respectively. For positive λ, as it is the case for PuO_2^{2+}, the figure also demonstrates that $g_{\parallel}$ is very close to 6 irrespective of the value of λ.

For $[PuO_2(NO_3)_3]^-$ and $[PuO_2(CO_3)_3]^{4-}$, the ϕ_u 5f are energetically split by the presence of the equatorial carbonate ligands. The CF parameter Γ and a reduced CF parameter $\gamma = \Gamma/\zeta$ are introduced in the model to take into account this splitting. The equatorial CF interaction couples the $5f_{\phi}$ orbitals as $\langle 3, \pm 1/2|\hat{H}^{CF}|-3, \pm 1/2\rangle = 1/2\Gamma$, breaking their degeneracy. As mentioned above, at the level of the 2-electron determinant wave functions the new contribution is from $^3\Pi_{\mp 2}$ ($m_{l1} = \mp 3$, $m_{l2} = \pm 2$). The corresponding model Hamiltonian is given in Equation S4 of the SI. The corresponding wave functions and g-factors are listed in Table 5. The fitting procedure to determine the CF model parameters from the ab initio calculations was not reliable because of correlations among the fit parameters. However, we can still investigate the g-factor dependence on the wave function composition depending on λ and γ. The resulting $g_{\parallel}$ as a function of the reduced CF parameters is displayed graphically in the bottom panel of Figure 2. As expected, the SO-free limits of free plutonyl are recovered when Γ tends to zero, with $g_{\parallel} = 6$ and 8 for finite positive or negative Λ,

dx.doi.org/10.1021/ic501168a | Inorg. Chem. 2014, 53, 8577−8592

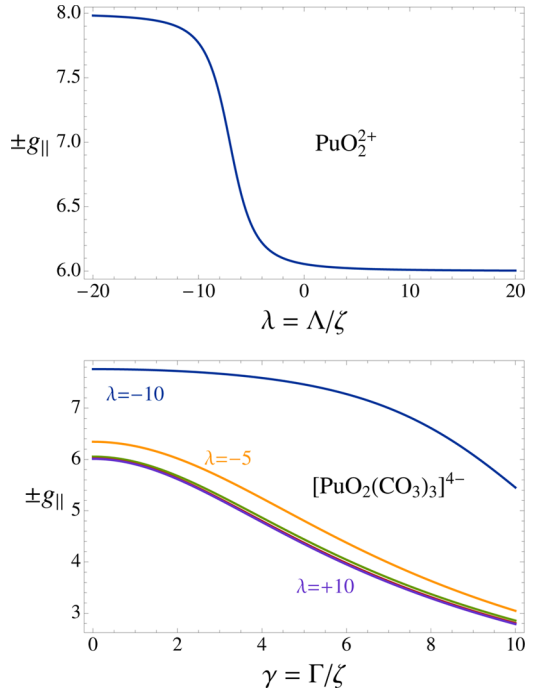

Figure 2. $g_{\|}$ for the ground state of $^3H_4$ parentage for free plutonyl (top) and for the carbonate complex (bottom), according to a CF + SO model. In the lower panel, $g_{\|}$ is plotted versus the equatorial reduced CF strength γ, with the reduced axial CF strength λ as a parameter.

respectively, and $\zeta \rightarrow 0$, corresponding to the SF $^3H_4$ and $^1\Gamma_4$ states. The effect of the new CF interaction is to reduce the magnitude of $g_{\|}$ as the energetic splitting between the two f_ϕ orbitals increases. EP already noted that the effect of SO coupling is apparently to increase $g_{\|}$, whereas the effect of the CF is to reduce $g_{\|}$, which is confirmed by the ab initio calculations and the CF models extracted from them. In the limit of very large CF splitting Γ and vanishing SO coupling, $g_{\|}$ tends to zero. In this case, we have $B = 0$, $A = -1/\sqrt{2}$ and $C = 1/\sqrt{2}$, the orbital angular momentum from the ϕ orbitals is quenched, and the combined spin and f_δ orbital magnetic moments cancel each other in the g-factor.

3.3. Electronic States from the Ab Initio Calculations.

The energies of the spin-free (SF) and spin−orbit (SO) states of the studied complexes have been calculated at the SCF-SF, SCF-SO, and the corresponding single-state PT2 levels, respectively, with three different active spaces. For the $5f^1$ complexes, the active spaces are labeled CAS(1,4) and CAS(7,10), corresponding to one electron in the 5f nonbonding ϕ and δ 5f orbitals, and CAS(1,4) augmented by the occupied and the antibonding σ and π orbitals with strong 5f metal character, respectively. Four states were computed when using the small active space and six with the large one. These active spaces have been recently used to describe the magnetic properties of neptunyl complexes and have allowed to properly (i) describe the nature of the ground and first excited states and (ii) reproduce the magnetic data.[30] CAS(1,4) is in essence a restricted open-shell Hartree−Fock calculation. For free UO_2^+, NpO_2^{2+}, and some NpO_2^{2+} complexes this computational level produces the correct physics and can be used for a simplified analysis, but it does not predict the correct ground state for $[UO_2(CO_3)_3]^{5-}$. The larger active space delivers better accuracy. For the $5f^2$ plutonyl species, the active spaces are labeled CAS(2,4) and CAS(8,10), and they include an equivalent set of active orbitals as used for the $5f^1$ systems but one more electron. Six triplet and 10 singlet states were computed when using the small active space, whereas 21 triplet and 28 singlet states were computed with the large one. The full set of data can be found in Tables S2−S8 of the SI. The main results obtained at the best level of calculation (i.e., PT2-SO with the large active space) are provided in Table 6 for NpO_2^{2+}, UO_2^+, $[NpO_2(CO_3)_3]^{4-}$, and $[UO_2(CO_3)_3]^{5-}$, and in Table 7 for PuO_2^{2+}, $[PuO_2(NO_3)_3]^-$ and $[PuO_2(CO_3)_3]^{4-}$, respectively.

Table 6. Relative Energies ΔE (cm^{-1}) and Assignment of Electronic States for the NpO_2^{2+}, UO_2^+, $[NpO_2(CO_3)_3]^{4-}$ and $[UO_2(CO_3)_3]^{5-}$ Complexes Calculated with Single-State CAS(7,10)PT2-SO[a]

	state	ΔE	composition
NpO_2^{2+}	$^2\Phi_{5/2u}$	0	88ϕ, 12δ
	$^2\Delta_{3/2u}$	3107	98δ, 2π
	$^2\Phi_{7/2u}$	8080	100ϕ
	$^2\Delta_{5/2u}$	9313	88δ, 12ϕ
UO_2^+	$^2\Phi_{5/2u}$	0	89ϕ, 11δ
	$^2\Delta_{3/2u}$	2616	97δ, 3π
	$^2\Phi_{7/2u}$	6679	100ϕ
	$^2\Delta_{5/2u}$	7889	89δ, 11ϕ
$[NpO_2(CO_3)_3]^{4-}$	$E_{3/2}$	0	95δ, 5π
	$E_{1/2}$	359	$56\phi_1$, 24δ, $20\phi_2$
	$E_{1/2}$	7103	71δ, $28\phi_1$, $1\phi_2$
	$E_{1/2}$	10 995	$80\phi_2$, $16\phi_1$, 4δ
$[UO_2(CO_3)_3]^{5-}$	$E_{3/2}$	0	93δ, 7π
	$E_{1/2}$	198	$56\phi_1$, $22\phi_2$, 22δ
	$E_{1/2}$	6067	73δ, $26\phi_1$
	$E_{1/2}$	8818	$78\phi_2$, $17\phi_1$, 5δ

[a]For additional results, see Tables S2−S5 in SI. The assigned state compositions in terms of the symmetries and occupations of the contributing 5f orbitals are given in percent.

Table 7. Relative Energies ΔE (cm^{-1}) and Assignment of Electronic States for the PuO_2^{2+}, $[PuO_2(NO_3)_3]^-$ and $[PuO_2(CO_3)_3]^{4-}$ Complexes Calculated with Single-State CAS(8,10)PT2-SO[a]

	Ω^b	ΔE	composition
PuO_2^{2+}	4_g	0	$95\,^3H_g$
	0_g^+	3132	$54\,^3\Sigma_g^-$, $29\,^3\Pi_g$, $15\,^1\Sigma_g^+$
	1_g	5464	$51\,^3\Pi_g$, $28\,^3\Sigma_g^-$, $18\,^1\Pi_g$
	5_g	7238	$99\,^3H_g$
	0_g^-	11 171	$100\,^3\Pi_g$
	1_g	11 628	$67\,^3\Sigma_g^- + 9\,^3\Pi_g + 21\,^1\Pi_g$
$[PuO_2(NO_3)_3]^-$	4	0	$91\,^3H$
	0^+	3017	$56\,^3\Sigma^-$, $23\,^3\Pi$, $15\,^1\Pi$
	1	4976	$31\,^3\Sigma^-$, $33\,^3\Pi$, $16\,^3H$, $14\,^1\Gamma$
	5	7868	$81\,^3H$
	0^-	11 406	$62\,^3\Pi$, $36\,^3H$
	1	11 850	$57\,^3\Sigma^-$, $15\,^3\Pi$, $24\,^1\Gamma$
$[PuO_2(CO_3)_3]^{4-}$	4	0	$88\,^3H$, $6\,^1\Gamma$
	0^+	2730	$57\,^3\Sigma^-$, $22\,^3\Pi$, $14\,^1\Sigma^+$
	1	4671	$33\,^3\Sigma^-$, $29\,^3\Pi$, $19\,^3H$, $13\,^1\Pi$
	5	8152	$77\,^3H$, $10\,^3\Sigma^-$, $10\,^3\Pi$
	0^-	11 459	$54\,^3\Pi$, $45\,^3H$
	1	11 881	$52\,^3\Sigma^-$, $18\,^3\Pi$, $25\,^1\Pi$

[a]For additional results see Tables S6−S8 in the SI. The assigned state compositions are given in percent. [b]The assignment of the SO states of $[PuO_2(NO_3)_3]^-$ and $[PuO_2(CO_3)_3]^{4-}$ refers to the dominant contribution from the corresponding free plutonyl $D_{\infty h}$ state.

dx.doi.org/10.1021/ic501168a | Inorg. Chem. 2014, 53, 8577−8592

Corresponding state level and interaction diagrams are shown in Figures 3 and 4. "First order" SO means SO interaction within a given nonrelativistic multiplet, whereas "second order" SO couples all calculated states.

For the free actinyl species, UO_2^+ and NpO_2^{2+}, the SO ground state is assigned as $^2\Phi_{5/2u}$ and mainly of $5f_\phi$ character. As shown in Figure 3, this state arises from the SO coupling of SF $^2\Phi_u$ and $^2\Delta_u$ wave functions. Therefore, the SO ground state affords a sizable admixture of δ character. The computed ratios of ϕ and δ character in the ground states of these actinyl ions, 89/11 for UO_2^+ and 88/12 for NpO_2^{2+}, are close to the composition of an idealized An $5f^1$ ion $|5/2, \pm 5/2\rangle$ state (86/14). The first excited

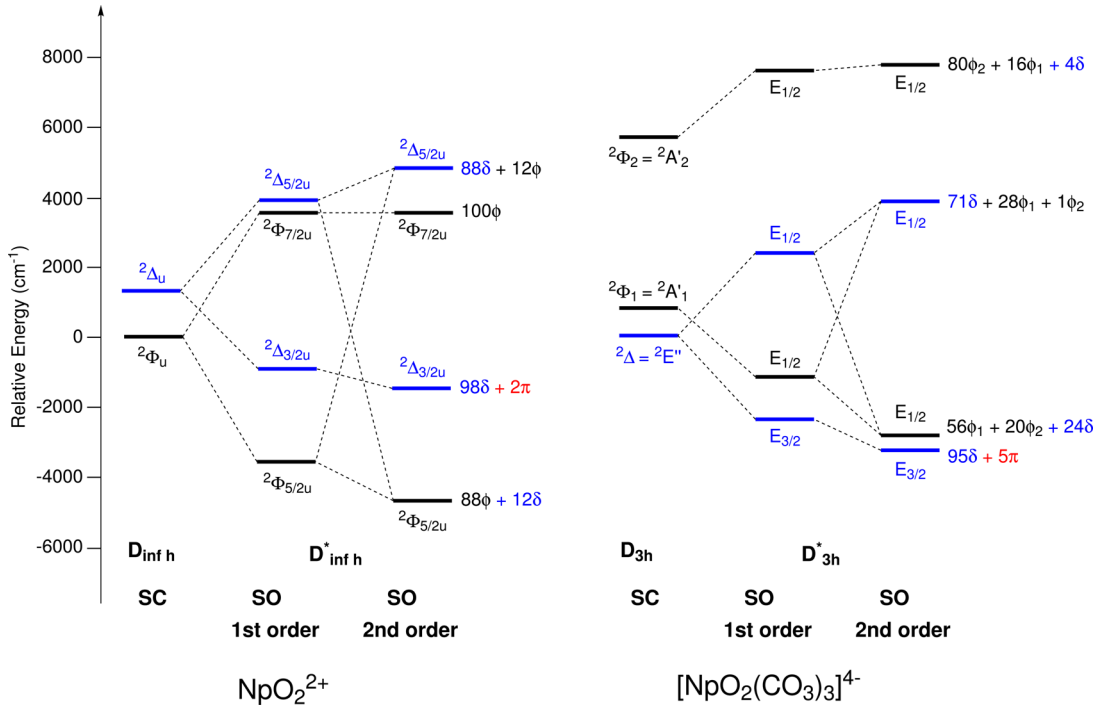

Figure 3. Energies and assignment of the lowest electronic states for NpO_2^{2+} and $[NpO_2(CO_3)_3]^{4-}$ from CAS(7,10)PT2 calculations. The $^2\Pi$ states are not shown because of their high energies. $E = 0$ corresponds to the SF ground state energy. The assigned state compositions at the SO level are given in percent. The corresponding diagrams for the U(V) systems are very similar and therefore not shown.

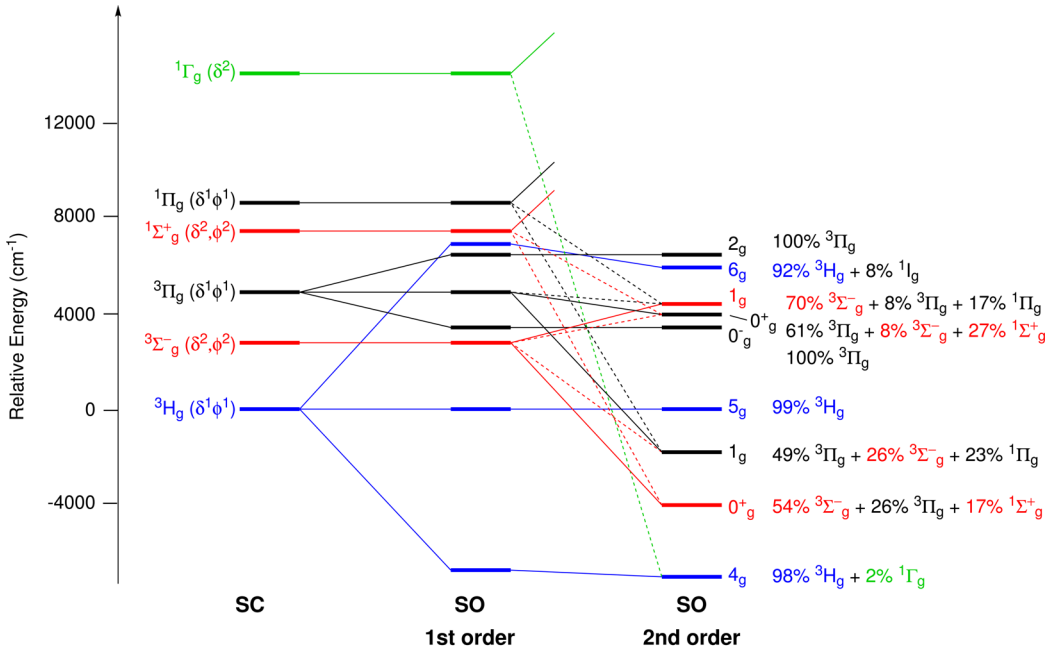

Figure 4. Energies and assignment of the lowest electronic states for PuO_2^{2+} from CAS(8,10)PT2 calculations. $E = 0$ corresponds to the SF ground state energy. The assigned compositions at the SO level are given in percent.

dx.doi.org/10.1021/ic501168a | Inorg. Chem. 2014, 53, 8577−8592

state $^2\Delta_{3/2u}$ is mainly of δ and formally of free-ion $|5/2, \pm 3/2\rangle$ parentage. However, as already pointed out in our previous work on NpO_2^{2+}, the composition of this state in the ab initio calculations strongly differs from the free-ion limit in that it has a very small π character (28% for $|5/2, \pm 3/2\rangle$ vs 2% from the CAS calculations). The strong energetic destabilization of the SF $^2\Pi$ states prevents an effective mixing of the $^2\Delta$ and $^2\Pi$ via SO coupling.

It is interesting to compare the relative energies of these states for the isolectronic uranyl(V) and neptunyl(VI) ions. The excited states in NpO_2^{2+} are computed at higher energy than in UO_2^{+}, relative to the ground state for each system. For example, the $^2\Delta_u$ excited state lies at 3107 cm^{-1} above the ground state in NpO_2^{2+}, whereas in UO_2^{+}, the same state is separated from the ground state by 2616 cm^{-1}. This observation is in agreement with previous studies performed on actinyl species.[51,53,66]

The SO ground state of the uranyl− and neptunyl−carbonate complexes corresponds at the CAS(7,10)PT2-SO level to states of $^2\Delta$ parentage ($E_{3/2}$), whereas the first excited state is of $^2\Phi$ parentage ($E_{1/2}$). As shown in Figure 3, because of the electrostatic repulsion by the equatorial carbonate ligands, the spin-free $^2\Phi_u$ state of the free actinyl ions are energetically destabilized and are split by the crystal field into two components $^2\Phi_1$ and $^2\Phi_2$, corresponding to the $^2A_1'$ and $^2A_2'$ species of the D_{3h} symmetry point group, with the $^2\Delta$ states below. At the SO level, the $^2\Delta$ states are split into $E_{1/2}$ and $E_{3/2}$ components, with the latter becoming the ground states in both systems. The first excited state $E_{1/2}$, separated from the ground states by 198 and 359 cm^{-1} for the uranyl− and neptunyl−carbonate complex, respectively, arises from SO coupling of $E_{1/2}$ states and affords strong admixtures of spin-free $^2\Phi_1$, $^2\Phi_2$, and $^2\Delta$ components. For example in $[NpO_2(CO_3)_3]^{4-}$, the first excited $E_{1/2}$ state at the SO level affords 56% $^2\Phi_1$, 20% $^2\Phi_2$, and 24% $^2\Delta$ character. The same state ordering was previously obtained for $[UO_2(CO_3)_3]^{5-}$ by Ruiperez et al.,[53] with an energetic separation of 119 cm^{-1} between the ground and first excited state.

This state ordering differs from the one previously described for the related nitrate complex $[NpO_2(NO_3)_3]^{-}$, where at the SO level the ground state is of $^2\Phi$ parentage and the first excited state, $E_{3/2}$ of $^2\Delta$ parentage, is 452 cm^{-1} higher in energy. This result must be attributed to a stronger destabilization of the SF Φ states by the carbonate ligands, which qualitatively agrees with the stronger electrostatic interactions noted in Table 2.

The ordering of the lowest spin-free and spin−orbit states in PuO_2^{2+} are shown in Figure 4. In agreement with Hund's rules, the ground state at the spin-free level for the plutonyl ion is the triplet ^3H_g, where the unpaired electrons occupy δ and ϕ orbitals with parallel angular momentum projections ($M_L = \pm 5 = \pm 3 \pm 2$) and spin and orbital angular momenta antiparallel. The SF ground state is well separated (by ≈3800 cm^{-1}) from the excited states of the 5f manifold (see Table S6). The first SF excited state is $^3\Sigma_g^-$, with ϕ and δ character. The second SF excited state is $^3\Pi_g$, involving ϕ and δ orbitals with antiparallel angular momentum projections ($M_L = 1 = \pm 3 \mp 2$). Spin-singlet excited states $^1\Sigma_g^+$, $^1\Pi_g$ and $^1\Gamma_g$ are found at energies $>10^4$ cm^{-1}.

At the SO level, the ground state of the PuO_2^{2+} ion remains predominantly in ^3H_g character, with $\Omega = 4_g$. SO coupling mixes states with the same Ω, and therefore, the ground state contains an admixture from the singlet state $^1\Gamma_g$, as discussed above in the context of the CF model. Because the energy gap between these states is large, the contribution of $^1\Gamma_g$ to the ground state is only 5%. The ^3H_g term is split by the SO interaction into three components, $\Omega = 4_g, 5_g$ and 6_g. The splitting is large and therefore other states are found energetically in between. At the CAS(8,10)PT2-SO level, the first excited state is computed at 3132 cm^{-1} above the ground state and has SF $^3\Sigma_g^-$ parentage with $\Omega = 0_g^+$. As a result of the SO interaction, this state contains strong admixtures from the SF $^3\Pi_g$ and $^1\Sigma_g^+$ states. The next excited states correspond to $\Omega = 1_g$ and 5_g at 5464 and 7238 cm^{-1} above the ground level, respectively. The same state ordering for PuO_2^{2+} below 10^4 cm^{-1} was previously obtained at different levels of theory.[50,66−69] For higher energies, the state ordering is sensitive to the level of theory used (i.e., the treatment of electron correlation and to spin−orbit coupling).

The state ordering for $[PuO_2(NO_3)_3]^{-}$ and $[PuO_2(CO_3)_3]^{4-}$ is similar to the plutonyl ion (see Tables S7 and S8). The SO ground state of the nitrate and carbonate complexes is dominantly of ^3H character, with a slight increase of the $^1\Gamma$ admixture relative to free plutonyl. Compared to free plutonyl, the first excited states corresponding to $\Omega = 0^+$ and 1 of the nitrate and carbonate species are energetically stabilized. The excited states with next higher energies correspond to $\Omega = 5, 0^-$, and 1 and are slightly destabilized instead.

3.4. Electronic *g*-Factors from the Ab Initio Calculations. The *g*-factors of the $5f^1$ and $5f^2$ complexes have been computed with SCF-SO and PT2-SO. The main results obtained with PT2-SO for the ground states and the first excited states are given in Tables 8 and 9 for the $5f^1$ and $5f^2$ systems, respectively. Additional data can be found in Tables S10 and S11 in the SI. We discuss absolute values of $g_\parallel$ and $g_\perp$ here.

According to the electronic state description given in section 3.3 and the corresponding CF models, the ground states of the free actinyl $5f^1$ species, UO_2^{+} and NpO_2^{2+}, are close to the free ion $|5/2, \pm 5/2\rangle$ limit. The calculated *g*-factors $g_\parallel \approx 4.22$ and $g_\perp = 0.00$ are likewise close to the free $5f^1$ ion limit where, for $|5/2, \pm 5/2\rangle$, one calculates $g_\parallel = 30/7 \approx 4.29$ and $g_\perp = 0$.

Table 8. Ground-State and First Excited-State *g*-Factors (Absolute Values) for NpO_2^{2+}, UO_2^{+}, $[NpO_2(CO_3)_3]^{4-}$, and $[UO_2(CO_3)_3]^{5-}$, from PT2-SO calculations[a]

active space	NpO_2^{2+}		UO_2^{+}		$[NpO_2(CO_3)_3]^{4-}$		$[UO_2(CO_3)_3]^{5-}$	
	$g_\parallel$	$g_\perp$	$g_\parallel$	$g_\perp$	$g_\parallel$	$g_\perp$	$g_\parallel$	$g_\perp$
				ground state				
(1, 4)	4.225	0.001	4.213	0.001	1.952	0.089	3.804	0.224
(7, 10)	4.233	0.002	4.222	0.001	2.070	0.013	2.118	0.015
				1st excited state				
(1, 4)	1.998	0.002	1.998	0.001	3.738	0.134	1.969	0.164
(7, 10)	2.037	0.005	2.058	0.002	3.784	0.111	3.873	0.173

[a]For CASSCF-SO results, see Table S10 in SI.

dx.doi.org/10.1021/ic501168a | Inorg. Chem. 2014, 53, 8577−8592

Table 9. Ground-State *g*-Factors (Absolute Values) for PuO_2^{2+}, $[PuO_2(NO_3)_3]^-$, and $[PuO_2(CO_3)_3]^{4-}$, from PT2-SO Calculations[a]

active space	PuO_2^{2+}		$[PuO_2(NO_3)_3]^-$		$[PuO_2(NO_3)_3]^{-b}$		$[PuO_2(CO_3)_3]^{4-}$	
	$g_\parallel$	$g_\perp$	$g_\parallel$	$g_\perp$	$g_\parallel$	$g_\perp$		
(2, 4)	6.041	0.000	5.855	0.000	5.897	0.000	5.764	0.000
(8, 10)	6.095	0.000	5.924	0.000	5.957	0.000	5.956	0.000

[a]For CASSCF-SO results see Table S11 in SI. [b]*g*-factors obtained with crystal embedding of the complex.[30]

Table 10. Spin and Angular Momentum Expectation Values for the Ground State Doublet Components with $\langle S_\parallel\rangle = \langle S_z\rangle > 0$, and *g*-Factors (Absolute Values), from PT2-SO Calculations

	$\langle L_\parallel\rangle$	$\langle L_\perp\rangle$	$\langle S_\parallel\rangle$	$\langle S_\perp\rangle$	$\lvert g_\parallel\rvert$	$\lvert g_\perp\rvert$
NpO_2^{2+}	−2.882	0.000	0.382	0.000	4.233	0.000
UO_2^+	−2.888	0.000	0.388	0.000	4.222	0.000
PuO_2^{2+}	−4.950	0.000	0.950	0.000	6.095	0.000
$[NpO_2(CO_3)_3]^{4-}$	−1.938	−0.012	0.451	0.003	2.070	0.013
$[UO_2(CO_3)_3]^{5-}$	−1.923	−0.012	0.431	0.002	2.118	0.015
$[PuO_2(NO_3)_3]^-$	−4.808	0.000	0.923	0.000	5.923	0.000
$[PuO_2(CO_3)_3]^{4-}$	−4.727	0.000	0.873	0.000	5.956	0.000

For the first excited state $^2\Delta_{3/2u}$, the calculations give $g_\parallel = 2.06$ and $g_\parallel = 2.04$ for UO_2^+ and NpO_2^{2+}, respectively, and $g_\perp = 0.00$. The corresponding *g*-factors for the $5f^1$ free-ion state $|5/2, \pm 3/2\rangle$ are $g_\parallel = 18/7 \approx 2.57$ and $g_\perp = 0.00$. The difference in $g_\parallel$ between the free ion value and the ab initio calculations is due to the small $^2\Pi$ characters of the first excited states in the latter, as already mentioned. The size of the active space has a very minor influence of the calculated *g*-factors for the f^1 actinyl ions.

The choice of active space has a stronger influence on the nature of the ground state, and hence on the *g*-factors, for the $5f^1$ actinyl tris-carbonate complexes. For $[UO_2(CO_3)_3]^{5-}$, the smallest active space, i.e. CAS(1,4), gives a ground state of $^2\Phi$ parentage ($E_{1/2}$) with $g_\parallel = 3.80$ and $g_\perp = 0.22$. The larger active space, CAS(7,10), gives a ground state of $^2\Delta$ parentage and $g_\parallel = 2.12$ and $g_\perp = 0.01$. Indeed, these *g*-factors are similar to those of the first excited state of UO_2^+, which has a similar assignment.

At the PT2-SO level, the ground state *g*-factors of $[NpO_2(CO_3)_3]^{4-}$ correspond to those of a state of $|5/2, \pm 3/2\rangle$ parentage, irrespective of the choice of the active space. However, the magnitude of the *g*-factors is mildly affected by the increase of the active space, with $g_\parallel$ increasing from 1.95 to 2.07 and $g_\perp$ decreasing from 0.09 to 0.01. The *g*-factors of the first excited state are characteristic of a state of $^2\Phi$ parentage with a larger magnetic anisotropy ($g_\parallel = 3.78$ and $g_\perp = 0.01$ for CAS(7,10)), and similar to the *g*-factors for the ground state of $[NpO_2(NO_3)_3]^-$- which also has D_{3h} symmetry.[30] We note in passing that that the *g*-factors of the nitrate complex were found to be rather insensitive to small changes of the Np−O_{yl} and Np−N distances, for instance, when optimizing the geometry with or without crystal embedding, and also not very sensitive to the active space as long as the state ordering remained intact. However, for a related $5f^1$ $[NpO_2Cl_4]^{2-}$ complex with D_{4h} symmetry, the *g*-factors are sensitive to geometric perturbations and to the active space size because of the system is close to an avoided state crossing.[30]

g-factors for the $5f^2$ plutonyl systems are given in Table 9. For free PuO_2^{2+}, the calculations give a parallel component $g_\parallel$ slightly above 6, and a perpendicular component of zero for both active spaces used. These values are close to the values expected for $^3H_{4g}$ (see also the CF section). In the SF state, the total orbital angular momentum $L_z = \pm 5$ is antiparallel to the total spin angular momentum $S_z = \mp 1$. The SO ground state is very close to this limit, which is confirmed by the calculations of the $\langle L_\parallel\rangle$ and $\langle S_\parallel\rangle$ expectation values (see Table 10 in section 3.5). Due to the SO coupling, the SO ground state contains a small admixture of the spin-free $^1\Gamma_{4g}$ state, leading to a small increase of the magnitude of the parallel component. This finding is reflected in the CF model of section 3.2.2.

The *g*-factors obtained for the coordinated plutonyl complexes $[PuO_2(NO_3)_3]^-$ and $[PuO_2(CO_3)_3]^{4-}$ are relatively close to those found for PuO_2^{2+} but lower in magnitude than what is possible for the free plutonyl ion due to the equatorial ligand interactions, as anticipated by the CF model in Figure 2. The largest active space gives $g_\parallel = 5.92$ and 5.95 for the nitrate and carbonate complex, respectively. The nature of the ground state (i.e., $^3H_4$) is not affected by the change of the active space, and the ground state remains well separated in energy from the first excited state. However, the increase of the active space leads to a slight decrease of the ^3H character in favor of $^1\Gamma$, which counteracts the effect from the equatorial CF in the magnitude of $g_\parallel$. Consequently, the parallel component of the *g*-factors of the plutonyl-nitrate and plutonyl-carbonate complexes slightly increases with the active space, from 5.85 to 5.92 for $[PuO_2(NO_3)_3]^-$ and from 5.76 to 5.95 for $[PuO_2(CO_3)_3]^{4-}$ when going from CAS(2,4) to CAS(8,10), respectively.

The computed *g*-factors of $[PuO_2(NO_3)_3]^-$ can be compared to experimental data. Bleaney, Llewellyn, and Pryce have characterized the *g*-factors of the nitrate complex diluted in an analogous diamagnetic uranyl(VI) host crystal.[70] In the same year, Hutchison and Lewis performed EPR measurements on the related complex $[PuO_2(C_2H_3O_2)_3]Na$.[71] The experimentalists reported $g_\parallel = 5.32$ for the nitrate complex and $g_\parallel = 5.92$ for the sodium acetate complex. The gas-phase calculations collected in Table 9 are in the range of the experimental *g*-factors, however, the computed gas-phase $g_\parallel$ of $[PuO_2(NO_3)_3]^-$ is very similar to the experimental value for the acetate complex and possibly overestimated. We note that the magnitude of $g_\parallel$ is slightly reduced at the SCF-SO level (SI). In order to investigate a potential influence of the crystal embedding on the experimental *g*-factors of this plutonyl complex, calculations with an embedding model were performed for $[PuO_2(NO_3)_3]^-$. For details, see ref 30. The results are listed in Table 9 next to the gas-phase data and show that the environment in the crystal has a very minor influence of the magnetic properties of the complex. Because the distance between Pu and the equatorial ligands is

dx.doi.org/10.1021/ic501168a | Inorg. Chem. 2014, 53, 8577−8592

likely somewhat overestimated by the DFT optimizations both for the nitrate and the carbonate complex, this would diminish the strength of the equatorial CF interactions and, per Figure 2, lead to an overestimation of $g_{\|}$. For verification, the electronic g-factors of $[PuO_2(CO_3)_3]^{4-}$ were calculated with the Pu−O_{eq} distances shortened by 0.05 Å relative to the optimized DFT structure. The equatorial contraction led to a decrease of the magnitude of $g_{\|}$ from 5.96 to 5.79, consistent with the model of Figure 2. A similar equatorial contraction of the nitrate complex reduced $g_{\|}$ from 5.92 to 5.87.

3.5. Spin Magnetization and Natural Orbitals. Natural orbitals (NOs) and natural spin orbitals (NSOs for spin projection axis z) of free UO_2^+, NpO_2^{2+}, and PuO_2^{2+} generated from the PT2-SO density and spin magnetization density matrices are shown in Figures 5 and 6, respectively. The f_δ and f_ϕ

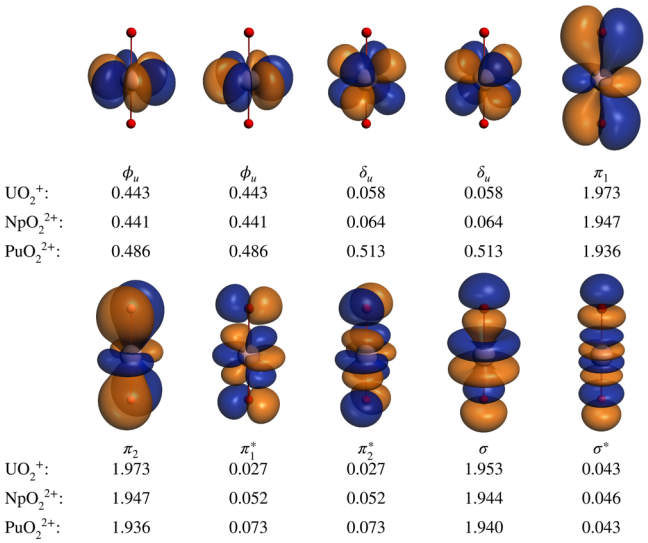

	ϕ_u	ϕ_u	δ_u	δ_u	π_1
UO_2^+:	0.443	0.443	0.058	0.058	1.973
NpO_2^{2+}:	0.441	0.441	0.064	0.064	1.947
PuO_2^{2+}:	0.486	0.486	0.513	0.513	1.936

	π_2	π_1^*	π_2^*	σ	σ^*
UO_2^+:	1.973	0.027	0.027	1.953	0.043
NpO_2^{2+}:	1.947	0.052	0.052	1.944	0.046
PuO_2^{2+}:	1.936	0.073	0.073	1.940	0.043

Figure 5. Selected NOs φ_p of NpO_2^{2+}, and the corresponding occupation numbers n_p of eq 1a for UO_2^+, NpO_2^{2+} and PuO_2^{2+}. PT2-SO ground states. Isosurface values: ± 0.03 au. The NO isosurfaces for UO_2^+ and PuO_2^{2+} appear very similar to those of NpO_2^{2+} and are therefore not shown (see SI instead).

NOs and NSOs appear essentially as textbook representations of nonbonding atomic 5f orbitals. The orbitals are so similar in appearance among the set of complexes that only the orbitals of NpO_2^{2+} (and $[NpO_2(CO_3)_3]^{4-}$ representing the carbonate complexes) are shown here, along with the occupations n_p and the contributions n_p^z to the "spin density" that are specific to each system. The full sets of figures are provided in the SI. Spatial degeneracy, leading to large orbital angular momentum, is represented by equivalent NOs with equal fractional populations, such as the f_ϕ and f_δ set in Figures 5 and 6 for the free actinyl ions. As a reminder, the n_p^z values for the NSOs add up to $2\langle S_z\rangle$. Here, $\langle S_z\rangle$ may differ from ±0.5 or ±1 for the f^1 and f^2 systems, respectively, due to SO coupling. For the ground state doublet of each system, we have chosen the components with $\langle S_z\rangle$>0 for the analysis.

The covalent interactions between the O_{yl} oxygen atoms and the actinide centers are clearly visible in the bonding and antibonding combinations of the f_σ and f_π orbitals. The magnitudes and the signs of the n_p^z for the spin magnetization z-component (corresponding to the spin density in the SF limit) are consistent with the CF model of section 3.2.1. For example, for the f^1 systems the f_ϕ components of the model wave functions

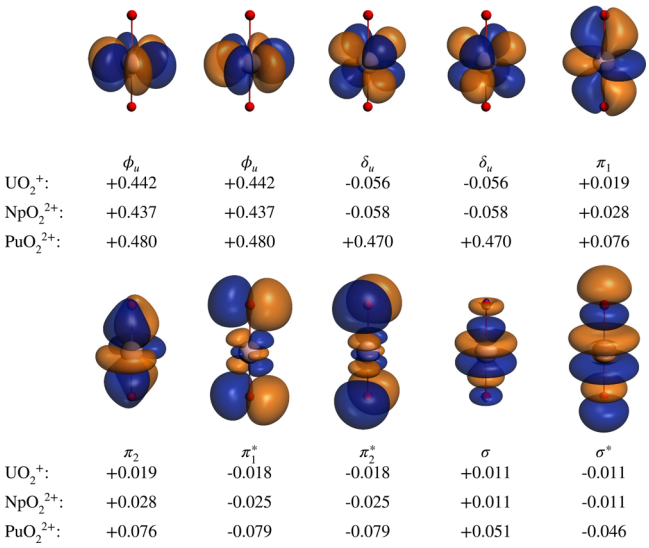

	ϕ_u	ϕ_u	δ_u	δ_u	π_1
UO_2^+:	+0.442	+0.442	-0.056	-0.056	+0.019
NpO_2^{2+}:	+0.437	+0.437	-0.058	-0.058	+0.028
PuO_2^{2+}:	+0.480	+0.480	+0.470	+0.470	+0.076

	π_2	π_1^*	π_2^*	σ	σ^*
UO_2^+:	+0.019	-0.018	-0.018	+0.011	-0.011
NpO_2^{2+}:	+0.028	-0.025	-0.025	+0.011	-0.011
PuO_2^{2+}:	+0.076	-0.079	-0.079	+0.051	-0.046

Figure 6. Selected NSOs of NpO_2^{2+} for the z-direction of the spin-magnetization, φ_p^z of eq 1b, and the corresponding n_p^z for UO_2^+, NpO_2^{2+} and PuO_2^{2+}. PT2-SO ground state components with $\langle S_z\rangle$>0. Isosurface values: ± 0.03 au. The NSO isosurfaces for UO_2^+ and PuO_2^{2+} appear very similar to those of NpO_2^{2+} and are therefore not shown (see SI instead).

(i.e., $|-3,+1/2\rangle$), are associated with the coefficient A in Table 3 and affords ↑ spin. This is reflected in the positive n_p^z for the $5f_\phi$ NSOs. The f_δ component of the model wave functions, $|-2,-1/2\rangle$ associated with the coefficient B, corresponds to ↓ spin, which is reflected in the negative n_p^z for the $5f_\delta$ NSOs. The contributions of positive n_p^z for f_ϕ and negative n_p^z for f_δ, driven by SO coupling, is also reflected in the spin expectation value $\langle S_{\|}\rangle \approx 0.38$, which is far from the ±0.5 for scalar doublet state components (see Table 10). Based on the NO occupations as well as the n_p^z for UO_2^+ and NpO_2^{2+}, about 88% of the unpaired electron density is associated with the f_ϕ orbitals. This value is in nice agreement with $A^2 \approx 89\%$ for the CF model wave functions from Table 4.

For PuO_2^{2+}, according to the assigned $^3H_{4g}$ ground state, there are both f_ϕ and f_δ spin orbitals occupied, and they should contribute with the same sign to $\langle S_z\rangle$. This is indeed seen in the NSO n_p^z values in Figure 6, with each of the ϕ and δ 5f orbitals contributing close to 1/2 electron to the total unpaired spin count. As already pointed out, the PuO_2^{2+} system is close to the SF limit, which is reflected in the n_p and n_p^z values. Indeed, the calculation gives $\langle L_z\rangle = -4.95$ and $\langle S_z\rangle = +0.95$, close to the SF limits for this state component which would be −5 and +1. These results are also consistent with the CF model which gave a contribution of the SF $^1\Gamma$ state to the PuO_2^{2+} model wave function of only 2%.

Figures 7 and 8 display the NOs and NSOs for the carbonate complexes $[UO_2(CO_3)_3]^{5-}$, $[NpO_2(CO_3)_3]^{4-}$, and $[PuO_2(CO_3)_3]^{4-}$. The corresponding plots for $[PuO_2(NO_3)_3]^-$ are given in Figures S11 and S12 in the SI. Relative to UO_2^+ and NpO_2^{2+}, the occupations of the f_ϕ orbitals in the carbonate complexes $[UO_2(CO_3)_3]^{5-}$ and $[NpO_2(CO_3)_3]^{4-}$ are close to zero, while the unpaired electron is now associated with the f_δ orbitals. These changes from the free actinyl to the carbonate system are consistent with the CF model of section 3.2 and the state assignments from section 3.3. Indeed, for the carbonate systems, the model wave function of the $^2\Delta$ parentage ground state corresponds to an admixture of f_δ ($|-2,+1/2\rangle$) and

dx.doi.org/10.1021/ic501168a | Inorg. Chem. 2014, 53, 8577−8592

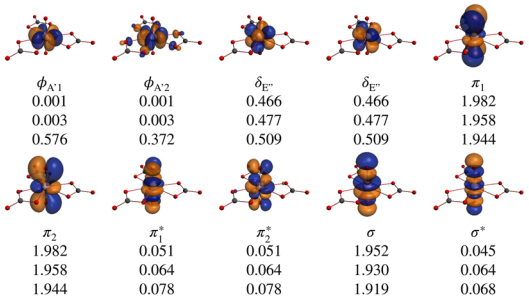

	$\phi_{A'1}$	$\phi_{A'2}$	$\delta_{E''}$	$\delta_{E''}$	π_1
$[UO_2(CO_3)_3]^{5-}$:	0.001	0.001	0.466	0.466	1.982
$[NpO_2(CO_3)_3]^{4-}$:	0.003	0.003	0.477	0.477	1.958
$[PuO_2(CO_3)_3]^{4-}$:	0.576	0.372	0.509	0.509	1.944

	π_2	π_1^*	π_2^*	σ	σ^*
$[UO_2(CO_3)_3]^{5-}$:	1.982	0.051	0.051	1.952	0.045
$[NpO_2(CO_3)_3]^{4-}$:	1.958	0.064	0.064	1.930	0.064
$[PuO_2(CO_3)_3]^{4-}$:	1.944	0.078	0.078	1.919	0.068

Figure 7. Selected NOs φ_p of $[NpO_2(CO_3)_3]^{4-}$, and occupation numbers n_p of eq 1a for the three carbonate complexes. PT2-SO ground states. Isosurface values: ± 0.03 au. The NO isosurfaces for $[UO_2(CO_3)_3]^{5-}$ and $[PuO_2(CO_3)_3]^{4-}$ appear very similar and are therefore not shown (see SI instead).

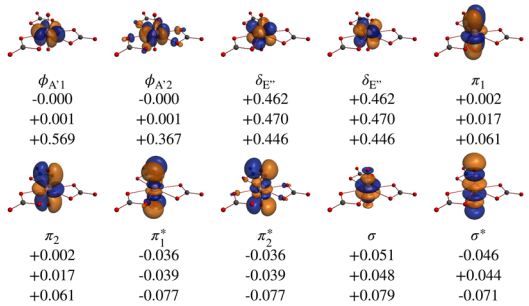

	$\phi_{A'1}$	$\phi_{A'2}$	$\delta_{E''}$	$\delta_{E''}$	π_1
$[UO_2(CO_3)_3]^{5-}$:	-0.000	-0.000	+0.462	+0.462	+0.002
$[NpO_2(CO_3)_3]^{4-}$:	+0.001	+0.001	+0.470	+0.470	+0.017
$[PuO_2(CO_3)_3]^{4-}$:	+0.569	+0.367	+0.446	+0.446	+0.061

	π_2	π_1^*	π_2^*	σ	σ^*
$[UO_2(CO_3)_3]^{5-}$:	+0.002	-0.036	-0.036	+0.051	-0.046
$[NpO_2(CO_3)_3]^{4-}$:	+0.017	-0.039	-0.039	+0.048	+0.044
$[PuO_2(CO_3)_3]^{4-}$:	+0.061	-0.077	-0.077	+0.079	-0.071

Figure 8. Selected NSOs of $[NpO_2(CO_3)_3]^{4-}$ for the z-direction of the spin-magnetization, φ_p^z of eq 1b, and the corresponding n_p^z for the three carbonate complexes. PT2-SO ground state component with $\langle S_z\rangle > 0$ for $[UO_2(CO_3)_3]^{5-}$, $[NpO_2(CO_3)_3]^{4-}$, and $[PuO_2(CO_3)_3]^{4-}$. Isosurface values: ± 0.03 au. The NSO isosurfaces for $[UO_2(CO_3)_3]^{5-}$ and $[PuO_2(CO_3)_3]^{4-}$ appear very similar and are therefore not shown (see SI instead).

f_π ($|-1,-1/2\rangle$) (Table 4) but with relatively small contributions from the latter.

In comparison, the $[PuO_2(CO_3)_3]^{4-}$ system remains closer to free PuO_2^{2+}, which is expected based on the state assignments and the results from the CF model. However, the D_{3h} crystal field breaks the degeneracy of the pair of $5f_\phi$ orbitals. This effects is readily apparent from the NO occupations and from the NSO n_p^z values for the carbonate complex in Figures 7 and 8 where the $\phi_{A'1}$ orbital now contributes significantly more to the unpaired spin and electron density than its $\phi_{A'2}$ partner. The pair of f_δ orbitals remains essentially degenerate in the NO occupations and the n_p^z, an assumption made when setting up the CF model.

A large imbalance of the occupations within either the ϕ or δ set of 5f orbitals due to a symmetry lowering from linear is indicative of a (partial) quenching of the orbital angular momentum. The reason is that a real "textbook" style 5f orbital as seen in the NO and NSO figures, which individually has no contribution to $\langle L_z\rangle$, is a linear combination of $|+m_l, m_s\rangle$ and $|-m_l, m_s\rangle$ functions with coefficients of equal magnitude. The reverse is also true, that is, if the calculation finds equal populations for the pair of $5f_\phi$ NOs, for example, it means that they can form a linear combination to give one of $|+3,m_s\rangle$ or $|-3,m_s\rangle$, which supports an orbital angular momentum—as in the case of the free actinyl species. For $[PuO_2(CO_3)_3]^{4-}$, the imbalance in the $\phi_{A'1}$ and $\phi_{A'2}$ occupations and n_p^z gives a relatively minor partial quenching of the angular momentum, as seen in Table 10 in the decrease of $\langle L_z\rangle = \langle L_\parallel\rangle$ from −4.95 for free PuO_2^{2+} to −4.73 for the carbonate complex. At the same time, SO coupling becomes stronger as seen by the decrease of $\langle S_z\rangle = \langle S_\parallel\rangle$ from +0.95 to +0.87 upon equatorial complexation. As orbital and spin angular momentum contribute with opposite signs to $g_\parallel$ for this state, the trends partially cancel. The situation is similar for the nitrate system where we already noted an overestimation of $g_\parallel$ compared to experiment.

3.6. Paramagnetic NMR. Calculating ligand NMR parameters of diamagnetic actinide complexes is already an interesting challenge.[72−74] The paramagnetism of open-shell complexes adds another layer of complexity.[75−78] The calculated g-factors and magnetic susceptibilities of the carbonate complexes $[UO_2(CO_3)_3]^{5-}$, $[NpO_2(CO_3)_3]^{4-}$, and $[PuO_2(CO_3)_3]^{4-}$ can be used in order to estimate paramagnetic effects on the NMR chemical shifts in the ligand sphere of these compounds. Experimental ^{13}C NMR spectra of actinyl carbonate complexes have been reported in the literature. Mizuoka et al. found that the ^{13}C NMR specta of a D_2O solution containing $[UO_2(CO_3)_3]^{5-}$ exhibits two sharp singlet peaks at 169.13 and 106.70 ppm at 273 K.[29] The peak at 169.13 ppm was attributed to the exchange between the free CO_3^{2-} and DCO_3^-, whereas the peak at 106.70 ppm was assigned to the coordinated CO_3^{2-} in the uranyl(V) carbonate complex. A ^{13}C shift around 170 ppm is also found for solutions of diamagnetic uranyl(VI) carbonate complexes. Clark et al. reported ^{13}C NMR spectra for neptunyl- and plutonyl-carbonate systems.[9] A single ^{13}C NMR resonance at 75.5 ppm (273 K) was assigned to the coordinated carbonate ligand of $[NpO_2(CO_3)_3]^{4-}$. For $[PuO_2(CO_3)_3]^{4-}$, the resonance was found at −210 ppm (295 K). Thus, compared to the free carbonate CO_3^{2-} and carbonate ligands of diamagnetic actinyl species, the paramagnetic actinyl-carbonate complexes exhibit pronounced changes in the ^{13}C ligand NMR shifts that increase dramatically with the number of unpaired electrons. Relative to carbonate, the paramagnetic ^{13}C shift δ^{pNMR} is −62, −93, and −376 ppm for $[UO_2(CO_3)_3]^{5-}$, $[NpO_2(CO_3)_3]^{4-}$, and $[PuO_2(CO_3)_3]^{4-}$, respectively.

The paramagnetic shift δ^{pNMR} is often given as the sum of two contributions, namely, a contact shift δ^C and a dipolar shift δ^D. The contact shift arises from unpaired spin density right at the NMR nucleus in question. This spin density is transmitted from the paramagnetic metal center to the ligands via covalent interactions. The dipolar shift arises from the magnetic field created by the magnetic moment of the metal center via through-space interaction with a ligand nuclear spin magnetic moment. In lanthanide (Ln) complexes, as a result of the inner shell character of the 4f orbitals and the mostly ionic Ln−ligand bonds, the contact shifts are often small. For actinide complexes, the interactions between the metal center and the ligands often involves a certain degree of covalency. However, in a first approximation, we consider the paramagnetic shifts δ^{pNMR} observed for the actinide−carbonate complexes to be dominated by the dipolar contribution. The isotropic δ^D that would be observed in solution can be estimated using the following equation proposed by Bertini et al.[75] for an axial system:

$$\delta^D = \frac{1}{12\pi R^3}(\chi_\parallel - \chi_\perp)(3\cos^2\theta - 1) \quad (4)$$

Here, R is the distance between the actinide center and the nucleus of interest and θ is the angle between the magnetic $\parallel = z = An-O_{yl}$ axis and the actinide−ligand distance vector. Further, $\chi_\parallel$ and $\chi_\perp$ are the axial and perpendicular principal components of the magnetic susceptibility tensor. The susceptibility

dx.doi.org/10.1021/ic501168a | Inorg. Chem. 2014, 53, 8577−8592

for the magnetic field in direction u has been given by van Vleck and can be written as[79]

$$\chi_u = \frac{1}{Q_0}\mu_0\mu_B^2 \sum_\lambda e^{-\beta E_\lambda}\left[\beta \sum_{a,a'} |\langle\psi_{\lambda a}|\hat{L}_u + g_e\hat{S}_u|\psi_{\lambda a'}\rangle|^2 + 2\sum_{\lambda'\neq\lambda}\sum_{a,a'} \frac{|\langle\psi_{\lambda a}|\hat{L}_u + g_e\hat{S}_u|\psi_{\lambda' a'}\rangle|^2}{E_{\lambda'} - E_\lambda}\right] \quad (5)$$

where the summation goes over the set of electronic states, with $\beta = 1/kT$ and $Q_0 = \sum_{\lambda,a} e^{-\beta E_\lambda}$. The indices a,a' count the components within degenerate states. The factors μ_0 and μ_B are the vacuum permeability and Bohr magneton, respectively. The implementation for χ in Molcas uses wave functions that diagonalize the Zeeman operator within the requested set of electronic states and then Boltzmann-averages the magnetization expectation values.[80] eq 5 represents a perturbation theoretical version of the approach, but we found that for our systems and for the active spaces used the results were numerically equivalent to adding all terms in eq (5) manually from $\hat{L}_u$ and $\hat{S}_u$ matrix elements and the state energies. For an electronic state that is energetically well separated from other states, ignoring zero-field splitting as we are dealing with $\tilde{S} = 1/2$ pseudospin ground states (having the SO interaction already included in the electronic wave functions), the relation between the susceptibility tensor components and the principal EPR g-factors was given by Bertini et al.[75] as

$$\chi_u = \mu_0\mu_B^2 g_u^2 \frac{\tilde{S}(\tilde{S}+1)}{3kT} \quad (6)$$

According to eq 4, large dipolar shifts may occur if the magnetic anisotropy at the metal center is large. Further, as long as $|g_\parallel| > |g_\perp|$, as is the case for our samples, the dipolar shifts for nuclei in the equatorial plane will be *negative* because $\chi_\parallel - \chi_\perp > 0$ while the geometric factor $3\cos^2\theta - 1 = -1$ is negative. As discussed in ref 76, using (6) in (4) leads to the same equation as when the paramagnetic dipolar NMR shift is calculated from the ab initio expression of Moon and Patchkovskii (MP),[78] if the hyperfine tensor in the MP expression is calculated assuming (i) a point magnetization distribution (a δ function) located at the metal center and (ii) the average electron magnetic moment vector components are given by $\mu_u = -\mu_B g_u \tilde{S}_u$ as discussed by Atherton[81] (with the molecular coordinate system coinciding with the principal axes of the g-tensor).

The calculated $\chi_\parallel$ and $\chi_\perp$ for $[UO_2(CO_3)_3]^{5-}$, $[NpO_2(CO_3)_3]^{4-}$, and $[PuO_2(CO_3)_3]^{4-}$ are collected in Table 11. As expected from the g-factors calculations detailed above, the magnetic anisotropy increases as follows: $[NpO_2(CO_3)_3]^{4-} < [UO_2(CO_3)_3]^{5-} < [PuO_2(CO_3)_3]^{4-}$. The reason for this trend is partially due to the state ordering. In both $[NpO_2(CO_3)_3]^{4-}$ and $[UO_2(CO_3)_3]^{5-}$, the SO ground state is of $^2\Delta$ parentage, which produces a smaller magnetic anisotropy than the states of $^2\Phi$ parentage. In light of the small energetic separation of the ground and first excited state in these systems, the contribution of the first excited state to the magnetic susceptibility is expected to be important at room temperature and lead to an increase of the magnetic anisotropy. This would be the case if we were to use a Boltzmann average of eq 6. However, magnetic coupling in the rightmost term of eq 5 of the $^2\Delta$ and $^2\Phi$ states is in fact responsible for the sizable $\chi_\perp$ listed in Table 11 for the $5f^1$ complexes, which keeps the δ^D at relatively modest magnitudes for the f^1 systems. In $[PuO_2(CO_3)_3]^{4-}$, the excited states are farther separated from the ground state and therefore do not contribute much to the magnetic susceptibility at room temperature. Here, the ground state is characterized by a large magnetic anisotropy with $g_\parallel = 5.95$ and $g_\perp = 0.00$, rendering this f^2 system more strongly paramagnetic than the f^1 counterparts in terms of the dipolar NMR shifts.

Table 11. Magnetic Susceptibility (cm^3 K mol^{-1}) and Calculated pNMR Dipolar Shifts (ppm) for $[NpO_2(CO_3)_3]^{4-}$, $[UO_2(CO_3)_3]^{5-}$, and $[PuO_2(CO_3)_3]^{4-}$[a]

complex	$\chi_\parallel T$[b]	$\chi_\perp T$[b]	δ^{D}[c]	δ^{D}[d]	expt δ^{pNMR}
$[NpO_2(CO_3)_3]^{4-}$	0.529	0.215	−25.99	−33.23	−93.5[e]
$[UO_2(CO_3)_3]^{5-}$	0.686	0.265	−32.08	−32.03	−62.43[e]
$[PuO_2(CO_3)_3]^{4-}$	3.332	0.042	−250.44	−253.21	−376[f]

[a]The experimental paramagnetic NMR shifts relative to carbonate ligands in a diamagnetic complex are given for comparison. [b]Magnetic susceptibility obtained using eq 5. 273 K for the Np and U complexes, 295 K for the Pu complex. [c]Dipolar shift obtained using eq 4 with the magnetic susceptibility. Temperatures as in footnote *b*. [d]Dipolar shift obtained using eq 4 with the magnetic susceptibiliy estimated from eq 6 with the ground state g-factors. Temperatures as in footnote *b*. [e]Measurement performed at 273 K. [f]Measurement performed at 295 K.

The dipolar shifts δ^D of $[UO_2(CO_3)_3]^{5-}$, $[NpO_2(CO_3)_3]^{4-}$ and $[PuO_2(CO_3)_3]^{4-}$ are given in Table 11 and are compared to the δ^{pNMR} shifts estimated from the experimental data. In agreement with the magnetic anisotropy trends, the magnitude of the negative δ^D increases as follows: $[NpO_2(CO_3)_3]^{4-} < [UO_2(CO_3)_3]^{5-} < [PuO_2(CO_3)_3]^{4-}$. In terms of sign and order of magnitude, the calculated dipolar NMR shifts are in-line with experiment, in particular regarding the large negative shift for the Pu system. Nonetheless, the computed δ^D underestimate the experimental δ^{pNMR} by 30, 67, and 125 ppm for $[UO_2(CO_3)_3]^{5-}$, $[NpO_2(CO_3)_3]^{4-}$ and $[PuO_2(CO_3)_3]^{4-}$, respectively. The deviations between the calculated dipolar and experimental δ^{pNMR} shifts might have different origins. For instance, the magnetic anisotropy depends of the nature of the ground state but it is also influenced by excited electronic states if they are very low in energy. Another reason for disagreement with experiment would be the presence of nonzero contact shifts.

In order to investigate the possibility of contact shifts to occur, the noncollinear spin densities, $s(\boldsymbol{r})$ of eq 2, were calculated for the ground state ($E_{3/2}$) and the first excited state ($E_{1/2}$) of $[UO_2(CO_3)_3]^{5-}$ and $[NpO_2(CO_3)_3]^{4-}$, and for the ground state of $[PuO_2(CO_3)_3]^{4-}$. Isosurface plots, and contour line plots in the equatorial ligand planes, are shown in Figure 9. For the $5f^1$ systems, due to the fact that for the SF δ orbitals the equatorial plane coincides with a nodal plane, the in-plane spin densities for the ground states are not large. However, because of SO coupling, the in-plane spin density is not zero. Significant contact shifts may also arise from a thermal population of the first excited state. Nonetheless, the contour diagrams indicate that the spin density around the carbons is potentially small. This conclusion is supported by a recent study of the equatorial interactions of uranyl with carbonate[59] which, despite some significant buildup of electron density between U and the ligand oxygens, has been characterized as dominantly ionic.

The spin densities at the ligand atoms will need to be investigated in more detail in a follow-up study for three reasons: (i) The active spaces employed in the CAS calculations are not sufficient in order to produce subtle effects from spin polarization in the carbonate ligands. That is, the plots in Figure 9 indicate small magnitudes of the spin density around the carbon atoms, but the calculations are not yet accurate enough to obtain the ^{13}C contact shifts quantitatively. (ii) Even small spin density

dx.doi.org/10.1021/ic501168a | Inorg. Chem. 2014, 53, 8577−8592

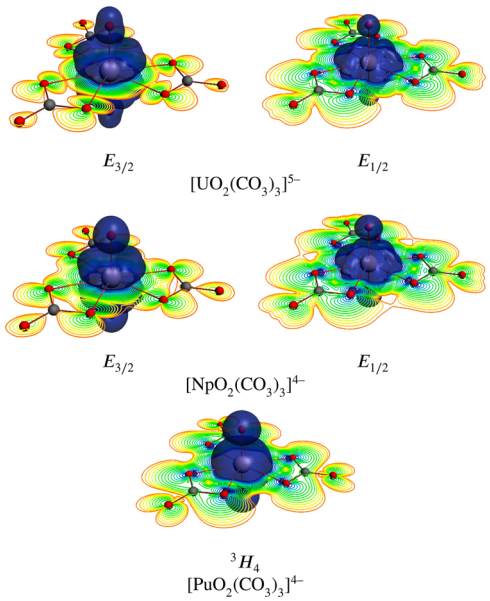

Figure 9. Noncollinear spin density *s* for the PT2-SO ground state (left) and the first excited state (right) for $[UO_2(CO_3)_3]^{5-}$ and $[NpO_2(CO_3)_3]^{4-}$, and for the ground state of $[PuO_2(CO_3)_3]^{4-}$. State components with $\langle S_z \rangle > 0$. Isosurfaces (±0.001 au) and in-plane contours.

accumulation at the ligand carbons may translate to sizable contact shifts.[82] (iii) For plutonyl, the ground state spin density around the metal center has large contributions from the $5f_\phi$ orbitals and therefore would allow for a transfer to the equatorial oxygens and further on to carbon via ligand σ orbitals. For this reason, we expect a more significant contribution from ^{13}C contact shifts. Tentatively, the bulk of the difference between the calculated dipolar shift and the observed paramagnetic effects in the NMR experiments are assigned to contact shifts.

4. CONCLUSIONS AND OUTLOOK

The magnetic behavior and the electronic state ordering of UO_2^+, NpO_2^{2+}, PuO_2^{2+}, and their tris-carbonate complexes, can be understood in chemically intuitive terms with the help of CF models derived from accurate SO ab initio wave function calculations. Further, the visualization of electron densities and spin-magnetization densities in terms of contributions from natural orbitals is instructive, as it distills the information about bonding and magnetic properties contained in complex wave functions into simple-to-interpret sets of numbers and images. Similar visualizations and analyses may also be useful in studies of magnetic properties and electronic structure of other heavy-element complexes (e.g., candidates for molecular magnets).

In terms of EPR *g*-factors and paramagnetic effects in the NMR spectrum, $5f^2$ plutonyl PuO_2^{2+} is significantly more paramagnetic than corresponding $5f^1$ systems with Np(VI) and U(V). The reason is that in the $\phi^1\delta^1$ ground state the resulting large total orbital angular momentum is only partially canceled by the magnetism from the total spin angular momentum. The agreement of the calculated *g*-factors of $[PuO_2(NO_3)_3]^-$ with available experimental data is similarly good as in our previous work[30] on the *g*-factors of $[NpO_2(NO_3)_3]^-$. The dipolar shifts in the NMR spectrum for the carbonate systems investigated in the present study agree in sign and order of magnitude with the experimentally observed paramagnetic effects but are too small overall, likely due to additional contact shifts that were not modeled.

Follow-up work will address the distribution of the spin density in the complexes in more detail in an attempt to model ligand hyperfine coupling constants and the paramagnetic effects on the ligand NMR chemical shifts more quantitatively. Already at the computational level employed in this work, the calculated spin density distributions show different magnitudes of unpaired spin around the actinide centers in the equatorial ligand planes of the carbonate ligands, depending on the nature of the electronic state. We also plan to replicate the experimentally observed temperature dependence of the carbon shifts[9] and investigate the validity of the point magnetic moment approximation underlying eq 4 versus calculating the dipolar hyperfine tensor explicitly from a spatially extended magnetization density.

■ ASSOCIATED CONTENT

Ⓢ Supporting Information

Additional data regarding the geometry optimizations, energies and assignment of electronic states for the studied complexes at the SCF, SCF-SO, and PT2-SO level, ground-state and first excited-state electronic *g*-factors at the SCF-SO level, composition of $|j,m_j\rangle$ spinors in terms of spherical harmonics and spin functions, model Hamiltonians, ERI parameters and details about the procedure used for the extraction of the CF parameters for PuO_2^{2+}, additional plots of orbitals and spin magnetization densities. This material is available free of charge via the Internet at http://pubs.acs.org.

■ AUTHOR INFORMATION

Corresponding Author

*E-mail: jochena@buffalo.edu.

Notes

The authors declare no competing financial interest.

■ ACKNOWLEDGMENTS

F.G., B.P., and J.A. acknowledge support from the U.S. Department of Energy, Office of Basic Energy Sciences, Heavy Element Chemistry program, under grant DE-FG02-09ER16066. We acknowledge the Center for Computational Research (CCR) at the University at Buffalo for providing computational resources. H.B. acknowledges support from the ANR grant ANR-09-BLAN-0195 TEMAMA.

■ REFERENCES

(1) *The Chemistry of the Actinide Elements*, 2nd ed.; Seaborg, G. T., Katz, J. J., Morss, L. R., Eds.; Kluwer: Dordrecht, 1986.
(2) *Transuranium Elements: A Half Century*; Morss, L. R., Fuger, J., Eds.; American Chemical Society: Washington, DC, 1992.
(3) *The Chemistry of the Actinide and Transactinide Elements*; Morss, L. R., Edelstein, N. M., Fuger, J., Katz, J. J., Eds.; Springer: Netherlands, 2006.
(4) Clark, D. L.; Neu, M. P.; Runde, W.; Keogh, D. W. In *Kirk-Othmer Encyclopedia of Chemical Technology*, 5th ed.; Seidel, A., Ed.; Wiley-Interscience: New York, 2007; Vol. 25
(5) Lukens, W. W.; Edelstein, N. M.; Magnani, N.; Hayton, T. W.; Fortier, S.; Seaman, L. A. *J. Am. Chem. Soc.* **2013**, *135*, 10742−10754.
(6) Minasian, S. G.; Keith, J. M.; Batista, E. R.; Boland, K. S.; Clark, D. L.; Kozimor, S. A.; Martin, R. L.; Shuk, D. K.; Tyliszczak, T. *Chem. Sci.* **2014**, *5*, 351−359.
(7) Gagliardi, L.; Roos, B. O. *Nature* **2005**, *433*, 848−851.
(8) Layfield, R. A. *Organometallics* **2014**, *33*, 1084−1099.
(9) Clark, D. L.; Hobart, D. E.; Neu, M. P. *Chem. Rev.* **1995**, *95*, 25−48.
(10) Efurd, D. W.; Runde, W.; Banar, J. C.; Janecky, D. R.; Kaszuba, J. P.; Palmer, P. D.; Roensch, F. R.; Tait, C. D. *Environ. Sci. Technol.* **1998**, *32*, 3893−3900.

(11) Ewing, R. C.; Runde, W.; Albrecht-Schmitt, T. E. *MRS Bull.* **2010**, *35*, 859−866.
(12) Kaltsoyannis, N. *Chem. Soc. Rev.* **2003**, *32*, 9−16.
(13) Kaltsoyannis, N.; Hay, P. J.; Li, J.; Blaudeau, J.-P.; Bursten, B. E. In *Chemistry of the Actinide and Transactinide Elements*; Katz, J. J., Morss, L. R., Edelstein, N., Fuger, J., Eds.; Springer: Netherlands, 2006.
(14) Autschbach, J.; Govind, N.; Atta-Fynn, R.; Bylaska, E. J.; Weare, J. H.; de Jong, W. A. In *Computational Methods in Lanthanide and Actinide Chemistry*; Dolg, M., Ed.; Wiley: New York, in press.
(15) Reiher, M.; Wolf, A. *Relativistic Quantum Chemistry. The Fundamental Theory of Molecular Science*; Wiley-VCH: Weinheim, 2009.
(16) Autschbach, J. *J. Chem. Phys.* **2012**, *136*, 150902.
(17) Case, D. A. *J. Chem. Phys.* **1985**, *83*, 5792.
(18) Arratia-Pérez, R.; Hernandez-Acevedo, L.; Malli, G. L. *J. Chem. Phys.* **2004**, *121*, 7743.
(19) Arratia-Pérez, R.; Malli, G. L. *J. Chem. Phys.* **2006**, *124*, 074321.
(20) Bolvin, H. *ChemPhysChem* **2006**, *7*, 1575−1589.
(21) Notter, F.-P.; Bolvin, H. *J. Chem. Phys.* **2009**, *130*, 184310.
(22) Verma, P.; Autschbach, J. *J. Chem. Theory Comput.* **2013**, *9*, 1052−1067.
(23) Verma, P.; Autschbach, J. *J. Chem. Theory Comput.* **2013**, *9*, 1932−1948.
(24) Autschbach, J.; Pritchard, B. *Theor. Chem. Acc.* **2011**, *129*, 453−466.
(25) Coutinho, J. T.; Antunes, M. A.; Pereira, L. C. J.; Bolvin, H.; Marçaloa, J.; Mazzanti, M.; Almeida, M. *Dalton Trans.* **2012**, *41*, 13568.
(26) Antunes, M. A.; Santos, I. C.; Bolvin, H.; Pereira, L. C. J.; Mazzanti, M.; Marçaloa, J.; Almeida, M. *Dalton Trans.* **2013**, *42*, 8861.
(27) Páez Hernández, D.; Bolvin, H. *J. Electron Spectrosc. Relat. Phenom.* **2014**, *194*, 74−80.
(28) Clark, D. L.; Hobart, D. E.; Palmer, P. D.; Sullivan, J. C.; Stout, B. E. *J. Alloys Compd.* **1993**, *193*, 94−97.
(29) Mizuoka, K.; Grenthe, I.; Ikeda, Y. *Inorg. Chem.* **2005**, *44*, 4472−4474.
(30) Gendron, F.; Páez-Hernández, D.; Notter, F.-P.; Pritchard, B.; Bolvin, H.; Autschbach, J. *Chem.—Eur. J.* **2014**, *20*, 7994−8011.
(31) te Velde, G.; Bickelhaupt, F. M.; Baerends, E. J.; van Gisbergen, S. J. A.; Fonseca Guerra, C.; Snijders, J. G.; Ziegler, T. *J. Comput. Chem.* **2001**, *22*, 931−967.
(32) Fonseca Guerra, C.; Snijders, J. G.; Te Velde, G.; Baerends, E. J. *Theor. Chem. Acc.* **1998**, *99*, 391.
(33) Baerends, E. J.; Ziegler, T.; Autschbach, J.; Bashford, D.; Bérces, A.; Bickelhaupt, F. M.; Bo, C.; Boerrigter, P. M.; Cavallo, L.; Chong, D. P.; Deng, L.; Dickson, R. M.; Ellis, D. E.; van Faassen, M.; Fan, L.; Fischer, T. H.; Fonseca Guerra, C.; Ghysels, A.; Giammona, A.; van Gisbergen, S. J. A.; Götz, A. W.; Groeneveld, J. A.; Gritsenko, O. V.; Grüning, M.; Gusarov, S.; Harris, F. E.; van den Hoek, P.; Jacob, C. R.; Jacobsen, H.; Jensen, L.; Kaminski, J. W.; van Kessel, G.; Kootstra, F.; Kovalenko, A.; Krykunov, M. V.; van Lenthe, E.; McCormack, D. A.; Michalak, A.; Mitoraj, M.; Neugebauer, J.; Nicu, V. P.; Noodleman, L.; Osinga, V. P.; Patchkovskii, S.; Philipsen, P. H. T.; Post, D.; Pye, C. C.; Ravenek, W.; Rodríguez, J. I.; Ros, P.; Schipper, P. R. T.; Schreckenbach, G.; Seldenthuis, J. S.; Seth, M.; Snijders, J. G.; Solà, M.; Swart, M.; Swerhone, D.; te Velde, G.; Vernooijs, P.; Versluis, L.; Visscher, L.; Visser, O.; Wang, F.; Wesolowski, T. A.; van Wezenbeek, E. M.; Wiesenekker, G.; Wolff, S. K.; Woo, T. K.; Yakovlev, A. L. *Amsterdam Density Functional, SCM, Theoretical Chemistry*; Vrije Universiteit: Amsterdam, The Netherlands. Website: http://www.scm.com.
(34) Baerends, E. J.; Branchadell, V.; Sodupe, M. *Chem. Phys. Lett.* **1997**, *265*, 481−489.
(35) van Lenthe, E.; Baerends, E. J.; Snijders, J. G. *J. Chem. Phys.* **1993**, *99*, 4597−4610.
(36) Becke, A. D. *J. Chem. Phys.* **1993**, *98*, 5648−5652.
(37) Pye, C. C.; Ziegler, T. *Theor. Chem. Acc.* **1999**, *101*, 396−408.
(38) Aquilante, F.; De Vico, L.; Ferré, N.; Ghigo, G.; Malmqvist, P.; Neogrády, P.; Pedersen, T. B.; Pitoňák, M.; Reiher, M.; Roos, B. O.; Serrano-Andrés, L.; Urban, M.; Veryazov, V.; Lindh, R. *J. Comput. Chem.* **2010**, *31*, 224−247.
(39) Wolf, A.; Reiher, M.; Hess, B. A. *J. Chem. Phys.* **2002**, *117*, 9215−9226.
(40) Roos, B. O.; Taylor, P. R.; Siegbahn, P. E. M. *Chem. Phys.* **1980**, *48*, 157.
(41) Andersson, K.; Malmqvist, P.-A.; Roos, B. O.; Sadlej, A. J.; Wolinski, K. *J. Phys. Chem.* **1990**, *94*, 5483.
(42) Malmqvist, P.-A.; Roos, B. O.; Schimmelpfennig, B. *Chem. Phys. Lett.* **2002**, *357*, 230.
(43) Heß, B. A.; Marian, C. M.; Wahlgren, U.; Gropen, O. *Chem. Phys. Lett.* **1996**, *251*, 365−371.
(44) Pritchard, B. *Calculation of Magnetic Properties of Paramagnetic Molecules*. Ph.D. Thesis, University at Buffalo, State University of New York, 2014.
(45) Chibotaru, L. F.; Ungur, L. *J. Chem. Phys.* **2012**, *137*, 064112.
(46) Van Wüllen, C. *J. Comput. Chem.* **2002**, *23*, 779−785.
(47) Ikeda-Ohno, A.; Tsushima, S.; Takao, K.; Rossberg, A.; Funke, H.; Scheinost, A. C.; Bernhard, G.; Yaita, T.; Hennig, C. *Inorg. Chem.* **2009**, *48*, 11779−11787.
(48) Ikeda, A.; Hennig, C.; Tsushima, S.; Takao, K.; Ikeda, Y.; Scheinost, A. C.; Bernhard, G. *Inorg. Chem.* **2007**, *46*, 4212−4219.
(49) Docrat, T. I.; Mosselmans, J. F. W.; Charnock, J. M.; Whiteley, M. W.; Collison, D.; Livens, F. R.; Jones, C.; Edmiston, M. J. *Inorg. Chem.* **1999**, *38*, 1879−1882.
(50) Clavaguéra-Sarrio, C.; Vallet, V.; Maynau, D.; Marsden, C. J. *J. Chem. Phys.* **2004**, *121*, 5312−5321.
(51) Su, J.; Schwarz, W. H. E.; Li, J. *Inorg. Chem.* **2012**, *51*, 3231−3238.
(52) Matsika, S.; Pitzer, R. M. *J. Phys. Chem. A* **2000**, *104*, 4064−4068.
(53) Ruipérez, F.; Danilo, C.; Réal, F.; Flament, J.-P.; Vallet, V.; Wahlgren, U. *J. Phys. Chem. A* **2009**, *113*, 1420−1428.
(54) Gagliardi, L.; Grenthe, I.; Roos, B. O. *Inorg. Chem.* **2001**, *40*, 2976−2978.
(55) Gagliardi, L.; Roos, B. O. *Inorg. Chem.* **2002**, *41*, 1315−1319.
(56) Craw, J. S.; Vincent, M. A.; Hillier, I. H. *J. Phys. Chem.* **1995**, *99*, 10181−10185.
(57) Hay, P. J.; Martin, R. L.; Schreckenbach, G. *J. Phys. Chem. A* **2000**, *104*, 6259−6270.
(58) Odoh, S. O.; Schreckenbach, G. *J. Phys. Chem. A* **2011**, *115*, 14110−14119.
(59) Vallet, V.; Wahlgren, U.; Grenthe, I. *J. Phys. Chem. A* **2012**, *116*, 12373−12380.
(60) Ziegler, T.; Rauk, A. *Inorg. Chem.* **1979**, *18*, 1558−1565.
(61) Ziegler, T.; Rauk, A. *Inorg. Chem.* **1979**, *18*, 1755−1759.
(62) Eisenstein, J. C.; Pryce, M. H. L. *Proc. R. Soc. London A* **1955**, *229*, 20−38.
(63) Matsika, S.; Zhang, Z.; Brozell, S. R.; Blaudeau, J.-P.; Wang, Q.; Pitzer, R. M. *J. Phys. Chem. A* **2001**, *105*, 3825−3828.
(64) Eisenstein, J. C.; Pryce, M. H. L. *Proc. R. Soc. London A* **1956**, *238*, 31−45.
(65) Notter, F.-P.; Dubillard, S.; Bolvin, H. *J. Chem. Phys.* **2008**, *128*, 164315.
(66) Infante, I.; Gomes, A. S. P.; Visscher, L. *J. Chem. Phys.* **2006**, *125*, 074301.
(67) Maron, L.; Leininger, T.; Schimmelpfennig, B.; Vallet, V.; Heully, J.-L.; Teichteil, C.; Gropen, O.; Wahlgren, U. *Chem. Phys.* **1999**, *244*, 195−201.
(68) La Machia, G.; Infante, I.; Raab, J.; Gibson, J. K.; Gagliardi, L. *Phys. Chem. Chem. Phys.* **2008**, *10*, 7278−7283.
(69) Danilo, C.; Vallet, V.; Flament, J.-P.; Wahlgren, U. *Phys. Chem. Chem. Phys.* **2010**, *12*, 1116−1130.
(70) Bleaney, B.; Llewellyn, P. M.; Pryce, M. H. L. *Philos. Mag.* **1954**, *45*, 991.
(71) Hutchison, C. A.; Lewis, W. B. *Phys. Rev.* **1954**, *95*, 1096.
(72) Schreckenbach, G. *Inorg. Chem.* **2002**, *41*, 6560−6572.
(73) Straka, M.; Kaupp, M. *Chem. Phys.* **2005**, *311*, 45−56.
(74) Aquino, F.; Govind, N.; Autschbach, J. *J. Chem. Theory Comput.* **2011**, *7*, 3278−3292.
(75) Bertini, I.; Luchinat, C.; Parigi, G. *Prog. Nucl. Magn. Reson. Spectrosc.* **2002**, *40*, 249−273.

(76) Autschbach, J.; Patchkovskii, S.; Pritchard, B. *J. Chem. Theory Comput.* **2011**, *7*, 2175−2188.
(77) Bagno, A.; Saielli, G. *Theor. Chem. Acc.* **2007**, *117*, 603−619.
(78) Moon, S.; Patchkovskii, S. In *Calculation of NMR and EPR Parameters. Theory and Applications*; Kaupp, M.; Bühl, M.; Malkin, V. G., Eds.; Wiley-VCH: Weinheim, 2004; pp 325−338.
(79) Van den Heuvel, W.; Soncini, A. *J. Chem. Phys.* **2013**, *138*, 054113.
(80) Vancoillie, S.; Neese, F.; Rulisek, L.; Pierloot, K. *J. Phys. Chem. A* **2009**, *113*, 6149−6157.
(81) Atherton, N. M. *Principles of Electron Spin Resonance*; Ellis Horwood series in physical chemistry Prentice Hall: New York, 1993.
(82) Pritchard, B.; Autschbach, J. *Inorg. Chem.* **2012**, *51*, 8340−8351.